Copper Transporter ATP7A Limits Vascular Inflammation and Aortic Aneurysm Development: Role of miR-125b

Varadarajan Sudhahar[1,2,5], Archita Das[1,2], Tetsuo Horimatsu[1,3], Dipankar Ash[1,3], Silvia Leanhart[1,5], Olga Antipova[7], Stefan Vogt[7], Bhupesh Singla[1,2], Gabor Csanyi[1,2], Joseph White[4], Jack H. Kaplan[6], David Fulton[1,2], Neal L. Weintraub[1,3], Ha Won Kim[1,3], Masuko Ushio-Fukai[1,3], Tohru Fukai[1,2,5]

[1]Vascular Biology Center, [2]Departments of Pharmacology and Toxicology, [3]Medicine (Cardiology), and [4]Pathology, Medical College of Georgia at Augusta University, Augusta, GA [5]Charlie Norwood Veterans Affairs Medical Center, Augusta GA, [6]Department of Biochemistry & Molecular Genetics, University of Illinois at Chicago, [7]X-ray Science Division, Argonne National Laboratory, Argonne, IL, USA

Running Title: Cu transporter ATP7A and Aortic Aneurysm Formation

Address correspondence to:
Tohru Fukai, M.D., Ph.D.
Vascular Biology Center
Department of Pharmacology and Toxicology
Medical College of Georgia at Augusta University
1460 Laney-Walker Blvd,
Augusta, GA 30912, USA
Phone: 706-721-6380
Email: tfukai@augusta.edu

ABSTRACT

Objective: Copper (Cu) is essential micronutrient and its dysregulation is implicated in aortic aneurysm (AA) development. The Cu exporter ATP7A delivers Cu via the Cu chaperone Atox1 to secretory Cu enzymes, such as lysyl oxidase (LOX), and excludes excess Cu. LOX is shown to protect against AA formation. However, the role and mechanism of ATP7A in AA pathogenesis remains unknown.

Approach and Results: Here we show that Cu chelator markedly inhibited angiotensin II (Ang II)-induced abdominal AA (AAA) in which ATP7A expression was markedly downregulated. Transgenic ATP7A overexpression prevented AngII-induced AAA formation. Conversely, Cu transport dysfunctional ATP7A$^{mut/+}$/ApoE$^{-/-}$ mice exhibited robust AAA formation and dissection, excess aortic Cu accumulation as assessed by X-ray fluorescence microscopy, and reduced LOX activity. In contrast, AAA formation was not observed in Atox1$^{-/-}$/ApoE$^{-/-}$ mice, suggesting that decreased LOX activity, which depends on both ATP7A and Atox1, was not sufficient to develop AAA. Bone marrow (BM) transplantation suggested importance of ATP7A in vascular cells, not BM cells, in AAA development. MicroRNA (miR) array identified miR125b as a highly upregulated miR in AAA from ATP7A$^{mut/+}$/ApoE$^{-/-}$ mice. Furthermore, miR125b target genes (histone methyltransferase Suv39h1 and the NFkB negative regulator TNFAIP3) were downregulated, which resulted in increased proinflammatory cytokine expression, aortic macrophage recruitment, MMP-2/9 activity, elastin fragmentation and vascular smooth muscle cell loss in ATP7A$^{mut/+}$/ApoE$^{-/-}$ mice and reversed by LNA-anti-miR125b infusion.

Conclusion: ATP7A downregulation/dysfunction promotes AAA formation via upregulating miR125b, which augments pro-inflammatory signaling in a Cu-dependent manner. Thus, ATP7A is a potential therapeutic target for inflammatory vascular disease.

INTRODUCTION

Abdominal aortic aneurysms (AAA) are a life-threatening condition occurring in up to 9% of elderly individuals (above 65 years old)[1, 2]. Although morphologically similar, ascending thoracic aortic aneurysms (TAA) and AAA represent distinct disease processes. TAA frequently result from a non-inflammatory process of medial degeneration including smooth muscle cell (VSMC) loss and elastin fragmentation[3]. Conversely, AAAs involve chronic aortic wall inflammation, extracellular matrix (ECM) degradation and compromised smooth muscle function[1, 2, 4] which causes weakening of the vessel wall and consequent progressive aortic dilation, rupture and death. Currently, the only form of treatment for AAA is endovascular or surgical repair, which is associated with significant procedural risks and complications[1, 2]. Therefore, understanding the cellular and molecular mechanisms underlying AAA progression is crucial to developing new, effective therapeutic strategies.

Copper (Cu), an essential micronutrient and catalytic cofactor, is involved in physiological processes such as wound repair, while excess Cu contributes to various inflammatory vascular diseases including atherosclerosis[5-7]. It has been shown that tissue Cu levels are significantly increased in pathological inflammatory conditions such as atherosclerosis and AA[8, 9]. Implanting a Cu cuff promotes neointima thickening in response to vascular injury[10], while Cu chelators prevent this response[11]. Cu also plays an important role in inflammatory responses involved in innate and adaptive immunity[7]. Cu deficiency alters intravascular adhesion of leukocytes to activated endothelial cells (ECs) and expression of adhesion molecules, such as ICAM-1/VCAM-1[12], while Cu chelators inhibit atherosclerosis and inflammation[13, 14]. However, the role of Cu in AAA development is unknown.

Since excess Cu is toxic, intracellular Cu levels are tightly controlled by Cu transport proteins[7, 15]. These include Cu importer CTR1, which uptakes and transports Cu through the plasma membrane [16]; Cu chaperone Antioxidant-1 (Atox1), which obtains Cu from CTR1 and delivers it to the Cu exporter ATP7A, which localizes at the trans-Golgi network (TGN) in the basal state. Then, ATP7A transports Cu to secretary Cu enzymes (e.g. lysyl oxidase (LOX))[7, 17, 18]. In pathological conditions in which excess Cu occurs, ATP7A translocates from the TGN to the plasma membrane to export the excess Cu to the extracellular space[18]. Thus, ATP7A is a key regulator of secretory Cu enzymes and intracellular Cu levels. X-linked loss-of-function mutation of ATP7A has been shown to cause Menkes disease in humans[19, 20]. Of note, global ATP7A knockout mice are embryonic lethal due to vascular defects [21]. Mice carrying the X-linked blotchy ATP7A mutation ($ATP7A^{mut/y}$ mice) have a splice site mutation introducing a new stop codon at amino acid residue 794 with an associated loss of Cu transport function. They survive more than 6 months of age[18, 22], and are a well characterized animal model to study the function of ATP7A in adult organisms. Using $ATP7A^{mut/y}$ mice, we previously reported that ATP7A plays an important role in VSMCs to regulate mesenteric arterial tone in hypertensive[23] and diabetic mice[24, 25]. Interestingly, hemizygous male blotchy $ATP7A^{mut/y}$ mice, but not heterozygous female blotchy $ATP7A^{mut/+}$ or control animals, had a progressive increase in the incidence of aneurysms with aging, primarily in the ascending aorta[26, 27]. However, the role and mechanisms for vascular ATP7A in AAA formation induced by Ang II infusion, which is an established AAA model [28], remains unclear.

MicroRNAs (miRs) are a family of ~22 nucleotide endogenous short noncoding RNAs which regulate gene expression either via translational inhibition or destabilization of target mRNAs.

Environmental chemicals such as heavy metals can interfere with the biogenesis and expression of miRNAs, leading to toxicological consequences. Changes in Cu concentrations can alter the expression of a diverse number of miRNAs in the olfactory system of zebrafish that are involved in signal transduction and other critical neurological processes[29]. Recent studies have shown that miRNAs play an important role in in AAA formation[30, 31]by regulating pathways including proteinases, extracellular matrix production, vascular cell homeostasis, and inflammation. Thus, it is possible that microRNAs might be involved in ATP7A-mediated aortic aneurysm development.

In the present study, we examined the role of ATP7A in Ang II-induced AAA formation using heterozygous ATP7A$^{mut/+}$/ApoE$^{-/-}$ mice, which have a normal life span, no spontaneous AAA formation, and reduced Cu transporter function, and the Cu chelator tetrathiomolybdate (TTM). We demonstrate that endogenous ATP7A protects against AAA formation by inhibiting vascular inflammation, MMP activity, elastin fragmentation and vascular apoptosis via limiting expression of pro-inflammatory miR-125b in a Cu-dependent manner. Thus, our results provide novel insights into the potential of ATP7A as a future therapeutic target for inflammatory vascular disease.

MATERIALS AND METHODS

The authors declare that all supporting data are available within the article and its online-only Data Supplement.

Animals: Heterozygous blotchy ATP7A mutant (ATP7A$^{mut/+}$) mice backcrossed to the C57BL/6J background, Atox1$^{-/-}$ mice on C57BL/6J background and heterozygous transgenic mice overexpressing ATP7A on C57BL/6J background were weaned at 4 weeks of age and maintained on normal laboratory diet (Teklad diet 2918) for 3 months. ApoE$^{-/-}$ mice were purchased from Jackson Laboratory (Stock No: 002052; Bar Harbor, Maine). ATP7A^{mut} mice carrying the X-linked blotchy ATP7A mutation have a splice site mutation introducing a new stop codon at amino acid residue 794 and show impaired copper transport function, but survive to more than 6 months of age[18, 22, 23]. ATP7A transgenic (ATP7A Tg) mice that overexpress the human ATP7A from the composite beta actin promoter (CAG) were generated[24,32]. ATP7A^{mut} or Atox1$^{-/-}$ or ATP7A Tg mice previously backcrossed into C57BL/6J genetic background for at least ten generations were crossed with ApoE$^{-/-}$ mice on C57BL/6J background to generate ATP7A^{mut}/ApoE$^{-/-}$, Atox1$^{-/-}$/ApoE$^{-/-}$ or ATP7A Tg/ ApoE$^{-/-}$ mice. ApoE$^{-/-}$ mice served as controls. The protocol for animal use was approved by Institutional Animal Care and Use Committee at Medical College of Georgia.

Experimental design and AAA Model: Mice were studied at 2-3 months old. Ang II (1000 ng/kg body weight/min; Cat# A2900, Sigma-Aldrich) was infused into the subcutaneous space in the interscapular area of female ApoE$^{-/-}$, ATP7A$^{mut/+}$/ApoE$^{-/-}$, or Atox1$^{-/-}$/ApoE$^{-/-}$ mice under parenteral anesthesia via Alzet osmatic mini pump (Alzet Model # 2004; Durect; Cupertino, CA, USA), as described previously[33]. For some experiments, male or female ApoE$^{-/-}$ or ATP7A Tg/ApoE$^{-/-}$ mice were continuously fed a high fat diet (HFD) (Diet # TD.88137; Harlan Teklad) containing 21% (wt/wt, which equals 42% kcal) saturated fat extracted from milk, 48.5% (wt/wt) carbohydrate, 17.3% (wt/wt) protein, and 0.2% (wt/wt) cholesterol (0.15% supplemented, and 0.05% from the fat source) during 4 weeks of Ang II infusion[28, 34, 35]. For TTM treatment, mice were randomly assigned and gavaged with water (control) or 0.7 mg/day/30g mice tetrathiomolybdate (TTM)

daily for 4 weeks, as described previously[13, 14, 36]. Ceruloplasmin activity was measured in the serum of mice before and after TTM treatment using a colorimetric assay based on substrate oxidation (Sigma, Cat# MAK177).

Aortic tissue samples were harvested at several time points over the aneurysm induction period (28 days in the Ang II model). The chest and abdominal cavities were opened, and blood was drawn from the right ventricle at the time of euthanasia. Aortas were perfused with cold PBS through the left ventricle. Using a dissection microscope, the periadventitial tissue was carefully dissected from the wall of the aorta. Aortic measurements were determined with a stage micrometer and optical eyepiece reticle. An aortic aneurysm (AA) was defined as an increase in the baseline outer diameter of 50%. The aneurysmal areas were removed, fixed in paraformaldehyde (4% (wt/vol) Cat#15712-S, Electron Microscopy Sciences) for immunohistochemistry, or snap frozen in liquid nitrogen, and then stored at –80°C for biochemical assays. Aneurysm severity was graded according to the following criteria[37, 38]: grade 1, remodeled tissue in the suprarenal region frequently containing thrombus; grade 2, pronounced bulbous form of grade 1 containing thrombus; grade 3, multiple aneurysms containing thrombus; or ruptured, ruptured aortic aneurysm.

Human aortic tissues sections: We purchased deidentified formalin fixed paraffin embedded (FFPE) sections of human AAA (n=3 males) and normal aortas (n=3 males) from Origene (Supplement Table V). Samples were used for immunohistochemical staining. The specificity of primary antibody was confirmed by negative control procedures, which gave consistently negative results.

Cell culture and transfection: Bovine aortic endothelial cells (BAEC; VEC Technologies) were grown in Dulbecco's modified Eagle's medium (DMEM) containing penicillin (100 U/ml), streptomycin (100 mg/ml), and 10% (vol/vol) fetal bovine serum and used for experiments until passage 10. Vascular smooth muscle cells (VSMC) were isolated from rat (RASM) and mouse (MASM) from thoracic aorta by enzymatic digestion as described previously[25].

Immunoblotting: For protein expression in aortic tissue, mice were perfused with cold phosphate buffer saline. Aortae were harvested, frozen in liquid nitrogen and then crushed and cells lysed with RIPA buffer (5 mM Tris-HCl (pH 7.6), 150 mM NaCl, 1% NP-40, 1%sodium deoxycholate, 0.1% SDS) containing protease inhibitor followed by brief sonication. Lysates were separated using SDS-polyacrylamide gel electrophoresis, transferred to nitrocellulose membranes, blocked in PBS containing 5% nonfat dry milk and 0.1% Tween 20, and incubated for overnight with primary antibodies. The following primary antibodies were used: anti-Atox1, anti-ATP7A, anti-Tubulin, anti-CCS, anti-Actin and anti-COX17. After incubation with secondary antibodies (Goat Anti-Rabbit IgG-HRP Conjugate, Bio-Rad, Goat Anti-Mouse IgG-HRP Conjugate, Bio-Rad), proteins were detected by ECL chemiluminescence.

Immunohistochemistry: Frozen sections were prepared by overnight 4% PFA incubation followed by sucrose dehydration and OCT embedding. Sections 7 μm in thickness were stained with antibodies against Mac3, CD45, MCP1, MMP2 or MMP9, incubated with biotin-conjugated anti-rat IgG antibody (Vector Laboratory) and visualized by VECTOR DAB following peroxidase labeling with VECTASTAIN Elite ABC Reagent (Vector Laboratories). Counterstaining with

hematoxylin was performed. Images were captured by an Axio scope microscope and processed by AxioVision 4.8 software. All positive stained cells were counted in at least 3 microscopic fields (x40). The results were expressed as number of positive cells/mm^2 area. Richard-Allan Scientific™ Elastic Stain (Thermo Scientific) was used for elastin staining. Elastin degradation was scored as described previously[39]. The grades were as follows: score 1, no degradation; score 2, mild elastin degradation; score 3, severe elastin degradation; and score 4, aortic rupture.

LOX activity assay. LOX activity in tissue lysates was measured by a high-sensitivity fluorescence assay, as previously described [40]. Aortic tissues were homogenized in 1X LOX Urea buffer and protein concentration was determined. Equal amounts of protein samples were incubated in the presence and absence of 500 μmol/L BAPN at 37 °C for 30 min with final reaction mixture supplied by Amplite Fluorimetric Lysyl Oxidase Assay kit (AAT Bioquest) per the manufacturer's instruction. The reaction was stopped on ice, and differences in fluorescence intensity (540-nm excitation wavelength and 590-nm emission wavelength) between samples with and without BAPN were determined.

Synchrotron X-ray Fluorescence Microscopy: Sections (5 μm thick) of formalin-fixed paraffin-embedded vascular tissues were prepared. For X-ray imaging, the sections were mounted intact on silicon nitride windows (area, 2 × 2 mm; thickness, 200 nm) manufactured by Silson (Cat# 11301147, Blisworth, U.K.) and attached by brief heating to 55°C, as previously described [40]. Specimens were imaged with the scanning X-ray fluorescence microprobe at beamline 2-ID-E of the Advanced Photon Source (Argonne, IL). Undulator-generated x-rays of 10-keV incident energy were monochromatized with a single bounce Si <111> monochromator and focused to a measured spot size of 0.3 x 0.5 μm using Fresnel zone plate optics. Sections were raster-scanned in steps of 4.0 μm, and fluorescence spectra were collected for 1- to 2-sec dwell times by using a single-element silicon drift detector (Vortex-EX, SII Nanotechnology, CA). Quantitation and image-processing of the X-ray fluorescence (XRF) data sets was performed with MAPS software. Quantitation of elemental content was achieved by fitting XRF spectra at each pixel, and comparing against a calibration curve derived from measurements of thin-film standards NBS-1832 and NBS-1833 (National Bureau of Standards, Gaithersburg, MD).

Quantitative Real Time-polymerase chain reaction: Total RNA was isolated from aorta using TRI reagent (Molecular Research Center, Inc) according to the manufacturer's instructions. 2 μg of total RNA were used to synthesize first stranded cDNA with a High-Capacity cDNA Reverse Transcription Kits. PCR was performed according to the manufacturer's protocol using ABI PRISM® 7000 Sequence Detection System 26 (Applied Biosystems, CA) and QuantiFast SYBR Green PCR Kit (Qiagen, CA). Amplification conditions were performed with a 5 min preincubation at 95°C, followed by 40 cycles of 10 s at 95°C and 30 s at 60°C. PCR products were subjected to melting curve analysis, using the ABI PRISM® 7000 Sequence Detection System, to exclude amplification of unspecific products. All real-time PCR primers were purchased from predesigned primers of QuantiTect primer assays (Qiagen). Results were normalized by 18S or HPRT expression levels.

Gelatin zymography for detection of MMP-2 and MMP-9: Protein was extracted from isolated abdominal aortas that had been snap frozen in liquid nitrogen and homogenized in a buffer containing 1 M NaCl, 2 M urea, 0.2 mM PMSF, 50 mM Tris (pH 7.4), 0.1% EDTA, 0.1% Brij-

35, and protease inhibitors (10 μg/ml aprotinin, 1 mM phenylmethylsulfonyl fluoride, 10 μg/ml leupeptin), as previously described[41]. Samples were sonicated on ice and centrifuged, and supernatants were used to quantify protein content. Protein lysate was placed in a nonreducing zymogram buffer (Cat#161-0764, Bio-Rad, Hercules, CA) and applied without boiling to a 10% zymogram gel (#161-1167, Bio-Rad). Gels were incubated in 2% Triton X-100 at room temperature for 30 min and then rinsed in H_2O for 5 min. Gels were incubated overnight at 37°C with gentle agitation in Zymogram developing buffer (Cat# 161-0766, Bio-Rad) containing 50 mM Tris-HCl, pH 7.5, 200 mM NaCl, 5 mM CaCl2, 0.02% Brij-35. Proteins were stained with Coomassie brilliant blue R-250 solution (Cat# 161-0436, Bio-Rad) and destained with a solution containing 40% methanol, 10% acetic acid, and 50% H_2O.

Immunofluorescence analysis: Frozen sections were prepared by overnight 4% PFA incubation followed by sucrose dehydration and OCT embedding. The tissue sections (7 μm) were incubated with blocking buffer (3%BSA in PBS) for 1 h. Next, the sections were incubated with anti-ATP7A (Sigma Aldrich) or anti-actin α-smooth muscle Cy3 (Sigma Aldrich) for 18 h at 4°C, rinsed in PBS/BSA, and then incubated in Goat Anti-IgY Antibody, FITC Conjugate (Genway) for 1 h at room temperature and rinsed with PBS. Tissue sections were mounted onto cover glass using Vectashield (Cat#H-1200, Vector Laboratories) and visualized using confocal microscopy.

TUNEL assay: TUNEL staining was carried out to detect apoptotic cells in aortic tissue using In Situ Cell Death Detection Kit according to the manufacturer's instructions (Cat#11684795910, Roche Diagnostics Co.)[42]. DAPI counterstaining was performed on aorta sections to label nuclei using VECTASHIELD mounting medium (Vector Laboratories). The number of TUNEL-positive nuclei per aortic section was normalized to total nuclei. Results are presented as percentage of apoptotic cells.

LNA-anti-miR-125b injection: Either locked nucleic acid (LNA)-anti-miR-125b or scrambled control-miR (miRCURY LNA miR inhibitor from Exiqon) was injected via retro-orbital approach at a concentration of 10 mg/kg. The mice were injected 1 day after AAA induction and were then given a weekly maintenance injection throughout the experiment period of 4 weeks. The sequenced of the LNA-anti-miRNA-125b was 5'-TCACAAGTTAGGGTCTCAGGGA-3'. The sequence of LNA scramble miR control was 5'-CATGTCATGTGTCACATCTCTT-3' as reported previously[43].

Quantitative PCR for miRNA and mouse inflammatory miRNA PCR array: Aorta were dissected, flash frozen using liquid nitrogen, and stored at -80C for processing. Total RNA was isolated using the Qiagen miRNeasy mini kit (cat #217004) according to the manufacturer's protocol. RNA concentrations were determined using the Nanodrop Spectrophotometer. RNA was then transcribed into cDNA using Qiagen miScript RT kit (cat#218161, Qiagen). miR-125b specific primer (cat #MS00005992, Qiagen) was used and samples were run on the Applied Biosystems 7900HT Real-Time PCR System with RNU6 as the control.

For the PCR array, RNA was isolated as described above. Small RNAs were retro-transcribed from 200 ng of total RNA using the miScript II RT kit (Qiagen). Then, reaction mixtures were pooled according to their specific group and added into Immunopathology miScript PCR array (Cat# MIMM-104ZA, Qiagen). The reaction was run according to the manufacturer's protocol. The expression of 84 mouse miRNAs predicted to regulate inflammatory genes was

assayed in this array. Data were analyzed using software provided by Qiagen specific to these assays (miScript miRNA PCR Array Data Analysis software in GeneGlobe Data Analysis Center), normalized to the average Ct of six snoRNA/snRNAs housekeeping miRNAs controls (SNORD61, SNORD68, SNORD72, SNORD95, SNORD96A, RNU6-2).

Statistical Analysis: Data are presented as mean ± SEM. Normality of the data (using Shapiro-Wilk test) and the equality of group variance (using Brown-Forsythe test) were performed on all data using SigmaPlot 14. Data were compared between groups of cells and animals by Student *t*-test when one comparison was performed or by ANOVA for multiple comparisons. When significance was indicated by ANOVA, the Tukey post-hoc test was used to specify between group differences. Values of *p<0.05, **p<0.01 and ***p<0.001 were considered statistically significant. Statistical tests were performed using Prism v4 (GraphPad Software, San Diego, CA).

RESULTS

Cu chelator TTM prevents AAA formation. To determine the role of Cu in AAA formation, we examined the effect of the Cu chelator tetrathiomolybdate (TTM) on AAA formation in Apo $E^{-/-}$ mice following Ang II infusion and a high fat diet (HFD), which recapitulates some of the pathological characteristics of AAA in humans[28, 34, 35]. Figure 1A shows that TTM significantly reduced AAA formation as assessed by maximal aortic diameter. The efficacy of TTM treatment to lower Cu status was confirmed by a reduction in activity of the serum Cu-dependent enzyme ceruloplasmin of 42% as assessed by its ferroxidase activity, which is an established surrogate maker of bioavailable Cu[13, 14, 36]. This finding suggests that excess Cu contributes to AAA formation induced by Ang II/HFD.

Reduction of ATP7A expression in human and mouse AAA tissues and inflamed vascular cells. Since ATP7A plays an important role in exporting excess Cu to maintain intracellular Cu homeostasis[7, 17, 18], we next examined ATP7A expression levels in the abdominal aorta from Ang II/HFD-induced AAA mice. Figure 1B and 1C show that ATP7A protein and mRNA expression were markedly reduced (P<0.05) in AAA aorta. Furthermore, immunofluorescence analysis showed a dramatic decrease of ATP7A expression in αSMA positive smooth muscle cell (SMC) layer and endothelial cell (EC) layer in AAA tissue compared to non-AAA tissue (Figure I in the Online-only Data Supplement). Reduction of ATP7A expression was also shown in aorta of AAA patients compared to non-AAA controls using immunostaining (Figure 1D). To address whether inflammation associated with AAA may be mechanistically linked to ATP7A downregulation, we examined the effects of inflammatory cytokines on ATP7A expression. We found that pro-inflammatory cytokines (TNFα, IL-1β and IL-6), which are involved in AAA pathology[44], significantly decreased ATP7A mRNA and protein expression in cultured ECs and vascular SMCs (VSMCs), without affecting expression of other pathways regulating copper metabolism (Figure 1E and Figure II in the Online-only Data Supplement). These data suggest that ATP7A expression is reduced in AAA in conjunction with inflammation.

Overexpression of ATP7A suppresses Ang II-induced AAA formation. To determine the functional significance of ATP7A in the formation of AAA, we examined the effects of overexpression of ATP7A on the development of Ang II/HFD-induced AAA using ATP7A overexpressing transgenic (Tg) mice[32], as we have previously described[24]. ATP7A overexpression significantly blunted the progression of AAA and related pathological changes (as discussed

below) induced by Ang II infusion (Figure 1F and Figure XI in the Online-only Data Supplement). These data suggest that the reduced ATP7A expression observed in AAA tissues may be linked to AAA pathogenesis.

ATP7A dysfunction accelerates AAA formation. To examine the protective role of endogenous ATP7A in AAA formation, we used X-linked blotchy ATP7A mutant mice[18, 22-24], which have a splice site mutation introducing a new stop codon at amino acid residue 794 with reduced Cu transport function[18, 22] and typically survive to more than 6 months of age[18, 22, 23]. Using the Ang II-induced AAA model without HFD, which produces a less severe AAA phenotype[28, 34, 35], we found that hemizygous male blotchy ATP7A$^{mut/y}$/ApoE$^{-/-}$ mice died within a week after Ang II infusion. Thus, we employed heterozygous female ATP7A$^{mut/+}$/ApoE$^{-/-}$ mice which had reduced Cu transport function without spontaneous AAA formation and age-matched female ApoE$^{-/-}$ (i.e. 2-3 month old) mice as a control. Of note, female control ApoE$^{-/-}$ mice exhibit much less incidences of AngII-induced AAA formation and inflammation than males, consistent with previous reports[45, 46]. There was no significant difference in blood pressure or serum cholesterol between ATP7A$^{mut/+}$/ApoE$^{-/-}$ mice and ApoE$^{-/-}$ mice following Ang II infusion (Figure III and IV in the Online-only Data Supplement). With saline infusion, AAA were not observed in either ATP7A$^{mut/+}$/ApoE$^{-/-}$ or ApoE$^{-/-}$mice (Figure V in the Online-only Data Supplement). However, Ang II infusion for 28 days markedly increased abdominal aortic dilation in ATP7A$^{mut/+}$/ApoE$^{-/-}$, as compared to ApoE$^{-/-}$ mice (Figures 2A and 2B). Of note, 35% (11/32) of Ang II-infused ATP7A$^{mut/+}$/ApoE$^{-/-}$ mice died versus 9% (2/23) of the ApoE$^{-/-}$ mice (Figure 2C). Moreover, ATP7A$^{mut/+}$/ApoE$^{-/-}$ mice exhibited a higher complexity of aneurysm pathology and dissection with thrombus as compared to control mice (Figure 2D and Figure VIA in the Online-only Data Supplement). Furthermore, ATP7A$^{mut/+}$/ApoE$^{-/-}$ mice exhibited significantly higher Cu levels in the AAA tissues as compared to ApoE$^{-/-}$ mice, as assessed by X-ray fluorescence microscopy (XFM)(Figure 2G).

ATP7A dysfunction in vascular cells, not bone marrow (BM) cells, contributes to AAA development. Since ATP7A is expressed in both BM cells and vascular cells[23, 47], we performed reciprocal BM transplantation (BMT) experiments to interrogate the functional importance of ATP7A expression in BM cells. For these BMT studies, heterozygous blotchy ATP7A$^{mut/+}$/ApoE$^{-/-}$, or WT ApoE$^{-/-}$ mice, were irradiated, followed by intravenous injection of BM (Figure VIIB in the Online-only Data Supplement). BMT studies confirmed the development of severe AngII-induced AAA formation in ATP7A$^{mut/+}$/ApoE$^{-/-}$ mice reconstituted with BM from WT ApoE$^{-/-}$ mice, while reconstitution of WT ApoE$^{-/-}$ mice with BM from ATP7A$^{mut/+}$/ApoE$^{-/-}$ mice did not alter AAA development. The mean maximal abdominal aortic diameter was 2.18 ± 0.15 mm in the ATP7A$^{mut/+}$/ApoE$^{-/-}$ mice reconstituted with ATP7A$^{mut/+}$/ApoE$^{-/-}$ BM, which was significantly greater than that of the WT ApoE$^{-/-}$ mice transplanted with ATP7A$^{mut/+}$/ApoE$^{-/-}$ BM (1.31 ± 0.02 mm) (Figure VIIA in the Online-only Data Supplement). Thus, these BMT studies suggest that ATP7A expression in vascular cells, but not BM cells, plays a critical role in transducing the AAA phenotype.

Impaired Atox1-ATP7A-LOX pathway is insufficient to induce AAA formation. ATP7A transports Cu to the secretory Cu enzyme pro-LOX for activity, which is essential for the crosslinking of collagen and elastin[48]. We thus examined if enhanced AAA formation in Cu transporter dysfunctional ATP7A mutant mice might be due to a decrease in LOX activity.

Previous studies have demonstrated that $LOX^{-/-}$ mice or mutant mice exhibit perinatal death from AA formation and spontaneous dissection[49], and that LOX mutant mice exhibit AAA characterized by fragmented elastin fibers and aberrant SMC layers[50]. Elastin van Gieson (EVG) staining of the aortas demonstrated enhanced degradation and disruption of aortic elastin in Ang II-induced AAA from $ATP7A^{mut/+}/ApoE^{-/-}$ mice compared with $ApoE^{-/-}$ mice (Figure 2E). Unexpectedly, deletion of Atox1 (Cu chaperone for ATP7A) in $ApoE^{-/-}$ mice, which reduced LOX activity to a similar extent as observed in $ATP7A^{mut/+}/ApoE^{-/-}$ mice (45-50% reduction) (Figure 2F), failed to enhance AngII-induced AAA (Figure 2A). These findings indicate that reduced LOX activity, induced by impaired Atox1-ATP7A pathway, alone is insufficient to promote AAA.

ATP7A dysfunction exacerbates vascular inflammation and matrix metalloproteinase (MMP) activity in Ang II-induced AAA mice: To investigate the mechanisms by which ATP7A dysfunction promotes Ang II-induced AAA formation, independent of LOX, we first examined the accumulation of inflammatory cells[4]. We found that accumulation of inflammatory cells including $Mac3^{+}$, MCP-1^{+} and $CD45^{+}$ cells (Figure 3A) as well as mRNA expression of pro-inflammatory genes (TNFα, IL-1β, MCP-1 and IL-6) and macrophage and adhesion molecules (CD68 and ICAM1), but not anti-inflammatory genes (such as arginase-1, IL-10) were significantly increased in the AAA region of $ATP7A^{mut/+}/ApoE^{-/-}$ mice compared to $ApoE^{-/-}$ mice (Figure 3B). By contrast, ATP7A-Tg/$ApoE^{-/-}$ mice exhibited a significant reduction in the expression of proinflammatory genes (Figure XI in the Online-only Data Supplement).

MMPs play a key role in the initiation and progression of AAA by promoting matrix degradation, thereby weakening the arterial wall and favoring aneurysm formation[4, 51, 52]. Since infiltrating inflammatory cells are major sources of MMPs[4, 51, 52], we measured MMP activity and expression in the aortas of Ang-II infused mice. Immunohistochemical analysis revealed that MMP2 and MMP9 protein expression (Figure 4A) and proteolytic activity (Figure 4B), which are known to contribute to ECM remodeling and aneurysm formation[4, 51, 52], were significantly increased in the arteries of $ATP7A^{mut/+}/ApoE^{-/-}$ mice compared to control $ApoE^{-/-}$ mice. These results indicate that ATP7 dysfunction exacerbates AAA formation by augmenting inflammatory cell accumulation and associated MMP activation.

ATP7A dysfunction increases VSMC loss in Ang II-induced AAA mice. Since loss of VSMC is a characteristic feature of AA formation[42, 53], we next examined VSMC density and apoptosis in the aorta of Ang II-infused mice. Immunofluorescence analysis of αSMA staining demonstrated that the VSMC density in the aortic media was significantly lower in $ATP7A^{mut/+}/ApoE^{-/-}$ mice as compared to $ApoE^{-/-}$ mice (Figure 4C). Furthermore, a significant increase in the number of apoptotic cells in the aortic wall, as measured by TUNEL, was seen in $ATP7A^{mut/+}/ApoE^{-/-}$ mice as compared to control $ApoE^{-/-}$ mice, indicating the enhanced apoptosis of vascular cells (Figure 4D). These results indicate that ATP7A dysfunction increases vascular apoptosis and decreases cell number of VSMCs, which may contribute to AAA formation. To examine if ATP7A knockdown in vascular cells directly induce apoptosis, we performed Annexin V-FITC and propidium iodide (PI) double staining using flow cytometry in cultured human VSMCs and ECs (Figure VIII in the Online-only Data Supplement). ATP7A knockdown in both cells did not induce early or late apoptotic cells and necrotic cells, compare to control cells (Figure VIII in the Online-only Data Supplement). Thus, vascular apoptosis increase in aorta of $ATP7A^{mut/+}/ApoE^{-/-}$ mice may be secondary due to the inflammatory cell accumulation.

ATP7A dysfunction augments miRNA-125b expression in aorta of Ang II-induced AAA mice. Given the involvement of miRNAs in AAA pathogenesis[30, 31], we examined whether miRNAs regulate the inflammatory response and AAA development induced by ATP7A dysfunction. We performed the miScript miRNA qPCR Array (Immunopathogenesis kit; Qiagen) in aortas from Ang II-infused ATP7A$^{mut/+}$/ApoE$^{-/-}$ and control ApoE$^{-/-}$ mice. We found that 3 of 88 miRNAs tested were upregulated at least 3- fold in aorta of Ang II-infused ATP7A$^{mut/+}$/ApoE$^{-/-}$ mice, as compared to control ApoE$^{-/-}$ mice, including the following miRNAs: miR-125b, miR-142a, miR-21a, (Figure 5A). Since miR-125b is a highly expressed miRNA and was reported to regulate proinflammatory gene expression in VSMC[54], we validated miR-125b expression using qPCR and confirmed that miRNA-125b was significantly upregulated in aortas of Ang II-infused ATP7A$^{mut/+}$/ApoE$^{-/-}$ mice (Figure 5B) as well as in VSMCs isolated from those aortas (Figure IX in the Online-only Data Supplement). These results suggest that ATP7A dysfunction increases miR-125b expression, which may in turn promote inflammation and AAA formation.

Anti-miRNA-125b Inhibits ATP7A dysfunction-induced acceleration of AAA formation. To determine the functional significance of miR-125b upregulation, we tested whether the anti-miR-125b can prevent ATP7A dysfunction-induced AAA formation in ATP7A$^{mut/+}$/ApoE$^{-/-}$ mice. We designed locked nucleic acid (LNA)-modified anti-miR-125b (LNA-Anti-miR-125b) to silence the expression of miR-125b *in vivo* and a control LNA-modified scrambled miR (scr-miR). Intravenous injection of LNA-anti miR-125b significantly inhibited the increase in aortic diameter (Figure 5C) and reduced miR-125b expression (Figure 5D) in Ang II-infused ATP7A$^{mut/+}$/ApoE$^{-/-}$ mice. Taken together, these results suggest that ATP7A dysfunction promotes AAA at least in part due to upregulation of miR-125b expression. Because inflammation and apoptosis are involved in AAA formation, we examined expression of miR-125b targeted inflammatory genes and anti-apoptotic genes in Ang II-infused ATP7A$^{mut/+}$/ApoE$^{-/-}$ mice treated with LNA-anti-miR-125b. Figure 5E shows that miR-125b targeted inflammatory genes (SUV39h1[54] or TNFAIP3[55]), but not anti-apoptotic genes (MCL-1, BCL-W, BCL-2[56]) were significantly decreased in Ang II-infused ATP7A$^{mut/+}$/ApoE$^{-/-}$ mice and rescued by anti-miR-125b treatment. Consistently, anti-miR-125b treatment significantly decreased inflammatory cell (Mac3) infiltration as well as expression of pro-inflammatory genes and adhesion molecules such as (IL-1β, IL-6, TNFa, MCP1, ICAM1) in aorta of ATP7A$^{mut/+}$/ApoE$^{-/-}$ mice (Figure 6A and 6B). Furthermore, anti-miR-125b also decreased MMP activity, elastin degradation, loss of VSMC density and vascular cell apoptosis in aortae of ATP7A$^{mut/+}$/ApoE$^{-/-}$ mice (Figure 6C, 6D, and Figure X in the Online-only Data Supplement). Collectively, these findings indicate that the hallmark features of the AAA phenotype seen in the dysfunctional aortas from ATP7A-ApoE$^{-/-}$ mice are due to miR-125b upregulation.

Role of ATP7A-miR125b pathway in AngII-induced AAA formation.
We next examined the expression of miR-125b in Ang II/HFD-induced AAA in which ATP7A expression was markedly downregulated (Figure 1B, 1C and Figure I in the Online-only Data Supplement) and found that miR-125b expression was increased in AAA aorta compare to control mice (Figure XIA and XIIA in the Online-only Data Supplement). Furthermore, ATP7A overexpression, which inhibited AAA formation (Figure 1F), reduced miR-125b upregulation induced by Ang II infusion (Figure XIA in the Online-only Data Supplement), suggesting the causal role of ATP7A downregulation in upregulation of miR-125b and AAA formation. Moreover, these mice showed increase of miR-125b target anti-inflammatory genes (SUV39h1[54] or TNFAIP3[55]), but not anti-apoptotic genes (MCL-1, BCL-W, BCL-2[56]), thereby reducing the

expression of pro-inflammatory genes and adhesion molecules (Figure XIB, XIC in the Online-only Data Supplement). Mechanistically, Cu chelator TTM treatment *in vivo* which inhibited AAA formation (Figure 1A) prevented upregulation of miR-125b induced by AngII infusion (Figure XIIA in the Online-only Data Supplement). Furthermore, ATP7A knockdown in cultured VSMCs increased miR125b expression, which was inhibited by TTM (Figure XIIB in the Online-only Data Supplement). Given that Cu exporter ATP7A dysfunction increased intracellular Cu level in vascular cells[19, 20, 57], these results suggest that ATP7A dysfunction-induced Cu elevation might contribute to miR-125b upregulation. Functional significance of miR-125b elevation was demonstrated by the observation that LNA-modified anti-miR-125b infusion significantly inhibited AAA formation induced by AngII/HFD. Furthermore, there was no additional preventive effect of ATP7A overexpression on anti-miR-125b-induced inhibitory effects on AAA formation, suggesting ATP7A-miR125b pathway is involved in AAA formation (Figure XIII in the Online-only Data Supplement). Taken together, these results suggest that decreased ATP7A expression in Ang II/HFD mice or ATP7A dysfunctional mutant mice may contribute to AAA formation mainly through Cu-dependent miR125b upregulation.

DISCUSSION

This study provides novel evidence that the Cu exporter ATP7A protects against AAA formation by suppressing inflammation and protecting vascular wall integrity (Figure 6E). Major findings in this study are as follows: 1) ATP7A expression is significantly reduced during AAA formation in AngII-infused mice and human AAA tissue; 2) the Cu chelator TTM, or ATP7A overexpression, prevented Ang II-induced AAA; 2) LOX activity was reduced to a similar extent in Cu transport dysfunctional ATP7A$^{mut/+}$/ApoE$^{-/-}$ mice and Cu chaperone deficient Atox1$^{-/-}$/ApoE$^{-/-}$ mice, but only the ATP7A$^{mut/+}$/ApoE$^{-/-}$ mice exhibited enhanced AAA formation and dissection, in association with Cu accumulation as assessed by XFM analysis; 3) ATP7A is a negative regulator of vascular inflammation and vascular apoptosis, which are involved in aneurysm formation; 4) BM transplantation experiments suggest that ATP7A expression in vascular cells, but not BM cells, plays an important role in AAA development; 5) augmented vascular miRNA-125b expression provides a novel mechanism that is responsible for increased vascular inflammation and subsequent apoptosis in the pathogenesis of AAA in ATP7A$^{mut/+}$/ApoE$^{-/-}$ mice and AngII/HFD ApoE$^{-/-}$ mice.

Cu chelator TTM which forms a tripartite TTM-copper-protein complex to chelates bioavailable Cu, has been used for the treatment of patients with Wilson disease who exhibit Cu toxicity [5, 6] and is shown to prevent atherosclerotic lesion development in ApoE$^{-/-}$ mice[14], acute inflammation and pulmonary fibrosis,[5-7, 13]. However, the effects of Cu chelation on AAA development have not been reported. Thus, to our knowledge, this is the first study to demonstrate that Cu chelator significantly inhibits Ang II/HFD-induced AAA formation. The efficacy of TTM in chelating Cu was confirmed by the reduced activity of serum secretory Cu enzyme ceruloplasmin, an established surrogate marker of bioavailable Cu[13, 36]. These findings suggest that excess Cu may contribute to AAA formation induced by Ang II/HFD. In the present study, we found that expression of Cu exporter ATP7A, but not Atox1, was significantly reduced in AAA tissues, which may result in excess accumulation of Cu in AAA. Of note, ATP7A protein was also downregulated in human AAA tissues compared to that of non-AAA, supporting the clinical significance of

ATP7A in AAA formation. Although the mechanism of downregulation of ATP7A in AAA tissues remains unclear, we found that inflammatory cytokines, which are involved in AAA pathology[44], induced decrease in ATP7A mRNA and protein expression in cultured VSMCs. Addressing underlying molecular mechanism in detail is the subject of future study. Moreover, functional significance of ATP7A downregulation was demonstrated by our observation that ATP7A overexpression in ApoE$^{-/-}$ mice mitigates Ang II/HFD-induced AAA formation. Together with Cu transport dysfunctional ATP7A^{mut} mice[18, 22], these findings indicate that endogenous ATP7A functions to protect against AAA formation. Thus, Cu chelation or restoring ATP7A expression may be potentially effective therapeutic option for the treatment of AAA in patients.

Using Ang II-induced AAA model without HFD, which produces a less severe AAA phenotype, we showed that hemizygous male blotchy ATP7A$^{mut/y}$/ApoE$^{-/-}$ mice died within seven days, while heterozygous female blotchy ATP7A$^{mut/+}$/ApoE$^{-/-}$ mice showed enhanced AAA formation and dissection with increased Cu accumulation, as compared to WT female ApoE$^{-/-}$ mice which showed the low incidence of AAA [45, 46]. It is shown that hemizygous blotchy ATP7A$^{mut/y}$ mice, but not heterozygous blotchy ATP7A$^{mut/+}$mice, spontaneously develop aneurysms, mostly in the ascending aorta, with an increased incidence with aging[26, 27]. Notably, Menkes disease patients, as well as hemizygous blotchy ATP7A$^{mut/y}$/ApoE$^{-/-}$ mice, also exhibit aneurysm formation in systemic arteries such as lumbar, iliac, splenic and hepatic arteries[58, 59]. Whether ATP7A limits aneurysm formation in arteries other than the aorta under various conditions such as hypertension, obesity or aging warrants future investigation. Furthermore, BMT experiments revealed that ATP7A in tissue-resident cells such as vascular cells such as VSMC and ECs plays an important role for preventing AAA development. VSMC loss is another key feature of human AAA that contributes to the degeneration of vascular wall integrity[42, 53]. The present study found that α-SMA staining as an index of VSMC density was markedly reduced, while apoptosis was highly increased, in the aortas of ATP7A dysfunctional mice. Furthermore, loss of EC integrity also contributes to AAA development in response to Ang II infusion[37]. Further studies are required to investigate the tissue specific role of ATP7A in VSMCs and ECs in limiting AAA formation.

LOX activity is essential for crossing of collagen and elastin, and loss of LOX activity is shown to lead to vascular dilation and rupture[49]. We thus examined whether AAA formation in ATP7A dysfunctional mutant mice could be due to either abnormal Cu absorption or reduced Cu transport to the secretory Cu-dependent enzyme pro-LOX (the precursor of LOX) [60] . Unexpectedly, we found that dysfunction of ATP7A, but not deficiency of Atox1 (Cu chaperone for ATP7A), augmented Ang II-induced AAA. Since both ATP7A dysfunction and Atox1 deficiency reduced LOX activity at the similar extent, these results indicate that the decreased LOX activity alone is insufficient to promote AAA. These findings also suggest that Atox1 and ATP7A may have distinct functions such that Atox1 functions as a Cu-dependent transcription factor [40, 61, 62] in addition to Cu chaperone for the ATP7A-LOX pathway[7]. Menkes disease is characterized by the extensive decrease in Cu levels in most tissues except for the kidney and small intestine due to abnormal Cu absorption in the intestine[19, 20]. Importantly, ATP7A dysfunctional mice exhibited increased Cu levels, as assessed by XFM analysis, in the AAA tissues. These results suggest that the reduced LOX activity in both strains of mice is not due to decreased tissue Cu levels. Consistent with this, cells isolated from Menkes patients show increased cellular Cu level due to a Cu efflux defect[19, 20]. Collectively, these results suggest that enhanced AAA formation in

ATP7A^{mut} mice is not simply due to a decrease in LOX activity, but to other (Cu-dependent) factors such as Cu-dependent transcription factor function of Atox1 as discussed below.

Inflammatory cell infiltration and proteolytic enzymes (MMPs) also contribute to AAA development in humans and animals. We found that inflammatory cell infiltration and expression/activity of MMP2 and 9 were significantly increased in the aorta of ATP7A$^{mut/+}$/ApoE$^{-/-}$ mice compared to control mice. As reported[51], infiltration of macrophages into the vessel wall presents a major source of MMPs and VSMC is also a major source of MMP2[52]. The increased MMPs promote matrix degradation, thus impairing the integrity of the arterial wall and promoting AAA development. We also found that transcription of pro-inflammatory genes, but not anti-inflammatory genes, was significantly increased in aorta with AAA from ATP7A$^{mut/+}$/ApoE$^{-/-}$ mice. There are two possible mechanisms underlying this response. First, Cu accumulation in ATP7A dysfunctional mice itself may promote vascular inflammation. For example, Cu was reported to induce IL-6 secretion in cultured cells,[63] while implantation of Cu coated discs in rats induced IL-6 production and recruitment of IL-1α-secreting cells[64]. Moreover, Cu chelation by TTM inhibited vascular inflammation and atherosclerosis in ApoE$^{-/-}$ mice[14]. Second, epigenetic regulation of inflammatory genes induced by ATP7A dysfunction may also contribute to vascular inflammation during AAA. Indeed, ATP7A$^{mut/+}$/ApoE$^{-/-}$ mice exhibit reduced expression of anti-inflammatory genes such as SUV39h1 and TNFAIP3, a negative regulator of NFkB[55]. Previous study reported dysregulation of Suv39h1 and associated chromatin H3K9me3 (which increases inflammatory gene expression) in VSMC of diabetic mice[54]. We recently reported that decreased ATP7A protein expression in diabetic mice contributed to endothelial dysfunction[25]. Thus, it is conceivable that ATP7A dysfunction may cause vascular inflammation via reducing the SUV39h1 and TNFAIP3 gene expression.

Inflammatory miRNAs also play an important role in AAA formation [30, 31]. The microRNA array and qPCR analysis in AAA tissues indicate that at least three inflammatory miRNAs (miR-125b, -142a and -21a) were significantly upregulated (more than 3-fold) in ATP7A dysfunctional mice as compared with control. Among them, we focused on miRNA-125b, since it is one of the highly expressed miRNAs involved in inflammation[54, 55] and also upregulated in the abdominal aorta from Ang II/HFD-induced AAA ApoE$^{-/-}$ mice. Previous studies also reported the upregulation of miR-125b in VSMCs isolated from human AAA samples compared to those from normal aortas[65]. Functional significance of miR-125b elevation was demonstrated by the evidence that LNA-modified anti-miR-125b treatment significantly prevented AngII/HFD-induced AAA formation. ATP7A overexpression had no additional inhibitory effects on anti-miR-125b-treated AngII/HFD mice, suggesting the ATP7A-miR125b pathway (Figure XIII in the Online-only Data Supplement). Of note, miR-125b is shown to repress SUV39h1[54] and TNFAIP3[55] as well as induces apoptosis in cancer cells by targeting anti-apoptotic Bcl-2, Bcl-W, and Mcl-1proteins[56]. In the present study, we found that LNA-anti-miR-125b treatment also rescued the decreased SUV39h1 and TNFAIP3 expression in ATP7A$^{mut/+}$ mice, which was associated with reduced inflammatory cytokine expression, aortic dilation, apoptosis and MMP activity without affecting anti-apoptotic genes. We also found that ATP7A dysfunction-induced Cu elevation was not sufficient to induce apoptosis in vascular cells. Given that vascular apoptosis is induced by pro-inflammatory cytokines [42, 53], it is tempting to speculate that the enhanced apoptosis in ATP7A^{mut}

mice via upregulating miR-125b may be due to the increased vascular inflammation during AAA formation.

Experiments using Cu chelator TTM suggest that decreased ATP7A expression in Ang II/HFD-induced or ATP7A dysfunction-induced AAA formation is mainly through the Cu-dependent miR125b-mediated inflammatory response. We previously reported that the Cu chaperone Atox1 functions as a Cu-dependent transcription factor to increase expression of the NADPH oxidase organizer p47phox in inflamed ECs, cyclin D1 and SOD3 in VSMCs or fibroblasts[7]. We found that the human, mouse or rat miR-125b promoter contains Atox1-binding sites (5'-GAAAGA-3'). Thus, it is likely that increased miR-125b expression in $ATP7A^{mut}$ mice could be mediated through Cu-dependent transcription factor function of Atox1. Addressing this point in detail and role of other microRNAs in AAA formation in $ATP7A^{mut}$ mice is the subject of future investigation.

In summary, we demonstrate that the Cu transporter ATP7A protects against AAA formation by limiting vascular inflammation and MMP activity, at least in part via suppressing pro-inflammatory miR-125b in a Cu-dependent manner (Figure 6E). Our studies provide novel insights into the Cu transporter ATP7A as a potential therapeutic target for treatment of vascular inflammatory diseases and reveal new complexities in the role of Cu-dependent processes in AAA development.

Acknowledgements

The US Department of Energy, Office of Science, Office of Basic Energy Sciences supported use of the Advanced Photon Source at Argonne National Laboratory, under contract No. DE-AC02-06CH11357. This research was supported by NIHR01HL070187 (to T.F.), Department of Veterans Affairs Merit Review grant 2I01BX001232 (to T.F.), NIHR01HL133613, NIHR01HL116976 (to T.F., M.U.-F.), NIHR01 HL135584 (to M.U.-F.), 15SDG25700406 (to V.S.), and HL124097, HL126949, HL134354 and AR070029 (to N.L.W), 17POST33660754 (to D.A.).

Authors' contributions

V.S. designed the study, performed experiments, analyzed data, and wrote the manuscript. A.D. D.A. T.H, S.L H. K. helped for preparing XFM sample and performed experiment, O.A, L.F. S.V. performed XFM experiment, B.S, G.C, J. W. provided non-AAA sample, J.H.K, D.F and N.W. gave suggestions to advance this project and edited manuscript. M.U.-F. and T.F. designed the overall study, analyzed data, and wrote, reviewed, and edited the manuscript. T.F. is the guarantor of this work and, as such, had full access to all the data in the study and takes responsibility for the integrity of the data and the accuracy of the data analysis.

Competing financial interests

The authors declare no competing financial interests.

REFERENCES

1. Nordon IM, Hinchliffe RJ, Loftus IM and Thompson MM. Pathophysiology and epidemiology of abdominal aortic aneurysms. *Nat Rev Cardiol*. 2011;8:92-102.
2. Weintraub NL. Understanding abdominal aortic aneurysm. *N Engl J Med*. 2009;361:1114-6.
3. Isselbacher EM. Thoracic and abdominal aortic aneurysms. *Circulation*. 2005;111:816-28.
4. Dale MA, Ruhlman MK and Baxter BT. Inflammatory cell phenotypes in AAAs: their role and potential as targets for therapy. *Arterioscler Thromb Vasc Biol*. 2015;35:1746-55.
5. Brewer GJ. Tetrathiomolybdate anticopper therapy for Wilson's disease inhibits angiogenesis, fibrosis and inflammation. *J Cell Mol Med*. 2003;7:11-20.
6. Brewer GJ. Anticopper therapy against cancer and diseases of inflammation and fibrosis. *Drug Discov Today*. 2005;10:1103-9.
7. Fukai T, Ushio-Fukai M and Kaplan JH. Copper transporters and copper chaperones: roles in cardiovascular physiology and disease. *Am J Physiol Cell Physiol*. 2018;315:C186-C201.
8. Koksal C, Ercan M, Bozkurt AK, Cortelekoglu T and Konukoglu D. Abdominal aortic aneurysm or aortic occlusive disease: role of trace element imbalance. *Angiology*. 2007;58:191-5.
9. Stadler N, Lindner RA and Davies MJ. Direct detection and quantification of transition metal ions in human atherosclerotic plaques: evidence for the presence of elevated levels of iron and copper. *Arterioscler Thromb Vasc Biol*. 2004;24:949-54.
10. Volker W, Dorszewski A, Unruh V, Robenek H, Breithardt G and Buddecke E. Copper-induced inflammatory reactions of rat carotid arteries mimic restenosis/arteriosclerosis-like neointima formation. *Atherosclerosis*. 1997;130:29-36.
11. Mandinov L, Mandinova A, Kyurkchiev S, Kyurkchiev D, Kehayov I, Kolev V, Soldi R, Bagala C, de Muinck ED, Lindner V, Post MJ, Simons M, Bellum S, Prudovsky I and Maciag T. Copper chelation represses the vascular response to injury. *Proc Natl Acad Sci U S A*. 2003;100:6700-5.
12. Schuschke DA, Saari JT and Miller FN. Leukocyte-endothelial adhesion is impaired in the cremaster muscle microcirculation of the copper-deficient rat. *Immunol Lett*. 2001;76:139-44.
13. Wei H, Frei B, Beckman JS and Zhang WJ. Copper chelation by tetrathiomolybdate inhibits lipopolysaccharide-induced inflammatory responses in vivo. *Am J Physiol Heart Circ Physiol*. 2011;301:H712-20.
14. Wei H, Zhang WJ, McMillen TS, Leboeuf RC and Frei B. Copper chelation by tetrathiomolybdate inhibits vascular inflammation and atherosclerotic lesion development in apolipoprotein E-deficient mice. *Atherosclerosis*. 2012;223:306-13.
15. Kim BE, Nevitt T and Thiele DJ. Mechanisms for copper acquisition, distribution and regulation. *Nat Chem Biol*. 2008;4:176-85.
16. Kaplan JH and Maryon EB. How Mammalian Cells Acquire Copper: An Essential but Potentially Toxic Metal. *Biophys J*. 2016;110:7-13.
17. Fukai T and Ushio-Fukai M. Superoxide dismutases: role in redox signaling, vascular function, and diseases. *Antioxid Redox Signal*. 2011;15:1583-606.
18. Lutsenko S, Barnes NL, Bartee MY and Dmitriev OY. Function and regulation of human copper-transporting ATPases. *Physiol Rev*. 2007;87:1011-46.
19. Mercer JF. The molecular basis of copper-transport diseases. *Trends Mol Med*. 2001;7:64-9.
20. Kaler SG. ATP7A-related copper transport diseases-emerging concepts and future trends. *Nat Rev Neurol*. 2011;7:15-29.

21. Wang Y, Zhu S, Weisman GA, Gitlin JD and Petris MJ. Conditional knockout of the Menkes disease copper transporter demonstrates its critical role in embryogenesis. *PLoS One*. 2012;7:e43039.
22. La Fontaine S, Firth SD, Lockhart PJ, Brooks H, Camakaris J and Mercer JF. Intracellular localization and loss of copper responsiveness of Mnk, the murine homologue of the Menkes protein, in cells from blotchy (Mo blo) and brindled (Mo br) mouse mutants. *Hum Mol Genet*. 1999;8:1069-75.
23. Qin Z, Gongora MC, Ozumi K, Itoh S, Akram K, Ushio-Fukai M, Harrison DG and Fukai T. Role of Menkes ATPase in angiotensin II-induced hypertension: a key modulator for extracellular superoxide dismutase function. *Hypertension*. 2008;52:945-51.
24. Sudhahar V, Urao N, Oshikawa J, McKinney RD, Llanos RM, Mercer JF, Ushio-Fukai M and Fukai T. Copper transporter ATP7A protects against endothelial dysfunction in type 1 diabetic mice by regulating extracellular superoxide dismutase. *Diabetes*. 2013;62:3839-50.
25. Sudhahar V, Okur MN, Bagi Z, O'Bryan JP, Hay N, Makino A, Patel VS, Phillips SA, Stepp D, Ushio-Fukai M and Fukai T. Akt2 Stabilizes ATP7A, a Copper Transporter for SOD3 (Extracellular Superoxide Dismutase), in Vascular Smooth Muscles: Novel Mechanism to Limit Endothelial Dysfunction in Type 2 Diabetes Mellitus. *Arterioscler Thromb Vasc Biol*. 2018.
26. Brophy CM, Tilson JE, Braverman IM and Tilson MD. Age of onset, pattern of distribution, and histology of aneurysm development in a genetically predisposed mouse model. *J Vasc Surg*. 1988;8:45-8.
27. Andrews EJ, White WJ and Bullock LP. Spontaneous aortic aneurysms in blotchy mice. *Am J Pathol*. 1975;78:199-210.
28. Daugherty A and Cassis LA. Mouse models of abdominal aortic aneurysms. *Arterioscler Thromb Vasc Biol*. 2004;24:429-34.
29. Wang L, Bammler TK, Beyer RP and Gallagher EP. Copper-induced deregulation of microRNA expression in the zebrafish olfactory system. *Environ Sci Technol*. 2013;47:7466-74.
30. Maegdefessel L, Dalman RL and Tsao PS. Pathogenesis of abdominal aortic aneurysms: microRNAs, proteases, genetic associations. *Annu Rev Med*. 2014;65:49-62.
31. Raffort J, Lareyre F, Clement M and Mallat Z. Micro-RNAs in abdominal aortic aneurysms: insights from animal models and relevance to human disease. *Cardiovasc Res*. 2016;110:165-77.
32. Ke BX, Llanos RM, Wright M, Deal Y and Mercer JF. Alteration of copper physiology in mice overexpressing the human Menkes protein ATP7A. *Am J Physiol Regul Integr Comp Physiol*. 2006;290:R1460-7.
33. Daugherty A, Manning MW and Cassis LA. Angiotensin II promotes atherosclerotic lesions and aneurysms in apolipoprotein E-deficient mice. *J Clin Invest*. 2000;105:1605-12.
34. Remus EW, O'Donnell RE, Jr., Rafferty K, Weiss D, Joseph G, Csiszar K, Fong SF and Taylor WR. The role of lysyl oxidase family members in the stabilization of abdominal aortic aneurysms. *Am J Physiol Heart Circ Physiol*. 2012;303:H1067-75.
35. Cassis LA, Gupte M, Thayer S, Zhang X, Charnigo R, Howatt DA, Rateri DL and Daugherty A. ANG II infusion promotes abdominal aortic aneurysms independent of increased blood pressure in hypercholesterolemic mice. *Am J Physiol Heart Circ Physiol*. 2009;296:H1660-5.
36. Pan Q, Kleer CG, van Golen KL, Irani J, Bottema KM, Bias C, De Carvalho M, Mesri EA, Robins DM, Dick RD, Brewer GJ and Merajver SD. Copper deficiency induced by tetrathiomolybdate suppresses tumor growth and angiogenesis. *Cancer Res*. 2002;62:4854-9.

37. Yoshioka K, Yoshida K, Cui H, Wakayama T, Takuwa N, Okamoto Y, Du W, Qi X, Asanuma K, Sugihara K, Aki S, Miyazawa H, Biswas K, Nagakura C, Ueno M, Iseki S, Schwartz RJ, Okamoto H, Sasaki T, Matsui O, Asano M, Adams RH, Takakura N and Takuwa Y. Endothelial PI3K-C2alpha, a class II PI3K, has an essential role in angiogenesis and vascular barrier function. *Nat Med*. 2012;18:1560-9.
38. Manning MW, Cassi LA, Huang J, Szilvassy SJ and Daugherty A. Abdominal aortic aneurysms: fresh insights from a novel animal model of the disease. *Vasc Med*. 2002;7:45-54.
39. Satoh K, Nigro P, Matoba T, O'Dell MR, Cui Z, Shi X, Mohan A, Yan C, Abe J, Illig KA and Berk BC. Cyclophilin A enhances vascular oxidative stress and the development of angiotensin II-induced aortic aneurysms. *Nat Med*. 2009;15:649-56.
40. Das A, Sudhahar V, Chen GF, Kim HW, Youn SW, Finney L, Vogt S, Yang J, Kweon J, Surenkhuu B, Ushio-Fukai M and Fukai T. Endothelial Antioxidant-1: a Key Mediator of Copper-dependent Wound Healing in vivo. *Sci Rep*. 2016;6:33783.
41. Kim HW, Blomkalns AL, Ogbi M, Thomas M, Gavrila D, Neltner BS, Cassis LA, Thompson RW, Weiss RM, Lindower PD, Blanco VM, McCormick ML, Daugherty A, Fu X, Hazen SL, Stansfield BK, Huo Y, Fulton DJ, Chatterjee T and Weintraub NL. Role of myeloperoxidase in abdominal aortic aneurysm formation: mitigation by taurine. *Am J Physiol Heart Circ Physiol*. 2017;313:H1168-h1179.
42. Yamanouchi D, Morgan S, Kato K, Lengfeld J, Zhang F and Liu B. Effects of caspase inhibitor on angiotensin II-induced abdominal aortic aneurysm in apolipoprotein E-deficient mice. *Arterioscler Thromb Vasc Biol*. 2010;30:702-7.
43. Ge Y, Sun Y and Chen J. IGF-II is regulated by microRNA-125b in skeletal myogenesis. *J Cell Biol*. 2011;192:69-81.
44. Juvonen J, Surcel HM, Satta J, Teppo AM, Bloigu A, Syrjala H, Airaksinen J, Leinonen M, Saikku P and Juvonen T. Elevated circulating levels of inflammatory cytokines in patients with abdominal aortic aneurysm. *Arterioscler Thromb Vasc Biol*. 1997;17:2843-7.
45. Alsiraj Y, Thatcher SE, Charnigo R, Chen K, Blalock E, Daugherty A and Cassis LA. Female Mice With an XY Sex Chromosome Complement Develop Severe Angiotensin II-Induced Abdominal Aortic Aneurysms. *Circulation*. 2017;135:379-391.
46. Henriques TA, Huang J, D'Souza SS, Daugherty A and Cassis LA. Orchidectomy, but not ovariectomy, regulates angiotensin II-induced vascular diseases in apolipoprotein E-deficient mice. *Endocrinology*. 2004;145:3866-72.
47. Qin Z, Konaniah ES, Neltner B, Nemenoff RA, Hui DY and Weintraub NL. Participation of ATP7A in macrophage mediated oxidation of LDL. *J Lipid Res*. 2010;51:1471-7.
48. Lucero HA and Kagan HM. Lysyl oxidase: an oxidative enzyme and effector of cell function. *Cell Mol Life Sci*. 2006;63:2304-16.
49. Maki JM, Rasanen J, Tikkanen H, Sormunen R, Makikallio K, Kivirikko KI and Soininen R. Inactivation of the lysyl oxidase gene Lox leads to aortic aneurysms, cardiovascular dysfunction, and perinatal death in mice. *Circulation*. 2002;106:2503-9.
50. Lee VS, Halabi CM, Hoffman EP, Carmichael N, Leshchiner I, Lian CG, Bierhals AJ, Vuzman D, Brigham Genomic M, Mecham RP, Frank NY and Stitziel NO. Loss of function mutation in LOX causes thoracic aortic aneurysm and dissection in humans. *Proc Natl Acad Sci U S A*. 2016;113:8759-64.
51. Keeling WB, Armstrong PA, Stone PA, Bandyk DF and Shames ML. An overview of matrix metalloproteinases in the pathogenesis and treatment of abdominal aortic aneurysms. *Vasc Endovascular Surg*. 2005;39:457-64.

52. Longo GM, Xiong W, Greiner TC, Zhao Y, Fiotti N and Baxter BT. Matrix metalloproteinases 2 and 9 work in concert to produce aortic aneurysms. *J Clin Invest*. 2002;110:625-32.
53. Lopez-Candales A, Holmes DR, Liao S, Scott MJ, Wickline SA and Thompson RW. Decreased vascular smooth muscle cell density in medial degeneration of human abdominal aortic aneurysms. *Am J Pathol*. 1997;150:993-1007.
54. Villeneuve LM, Kato M, Reddy MA, Wang M, Lanting L and Natarajan R. Enhanced levels of microRNA-125b in vascular smooth muscle cells of diabetic db/db mice lead to increased inflammatory gene expression by targeting the histone methyltransferase Suv39h1. *Diabetes*. 2010;59:2904-15.
55. Kim SW, Ramasamy K, Bouamar H, Lin AP, Jiang D and Aguiar RC. MicroRNAs miR-125a and miR-125b constitutively activate the NF-kappaB pathway by targeting the tumor necrosis factor alpha-induced protein 3 (TNFAIP3, A20). *Proc Natl Acad Sci U S A*. 2012;109:7865-70.
56. Gong J, Zhang JP, Li B, Zeng C, You K, Chen MX, Yuan Y and Zhuang SM. MicroRNA-125b promotes apoptosis by regulating the expression of Mcl-1, Bcl-w and IL-6R. *Oncogene*. 2013;32:3071-9.
57. Hamza I, Prohaska J and Gitlin JD. Essential role for Atox1 in the copper-mediated intracellular trafficking of the Menkes ATPase. *Proc Natl Acad Sci U S A*. 2003;100:1215-20.
58. Adaletli I, Omeroglu A, Kurugoglu S, Elicevik M, Cantasdemir M and Numan F. Lumbar and iliac artery aneurysms in Menkes' disease: endovascular cover stent treatment of the lumbar artery aneurysm. *Pediatr Radiol*. 2005;35:1006-9.
59. Mentzel HJ, Seidel J, Vogt S, Vogt L and Kaiser WA. Vascular complications (splenic and hepatic artery aneurysms) in the occipital horn syndrome: report of a patient and review of the literature. *Pediatr Radiol*. 1999;29:19-22.
60. Rowe DW, McGoodwin EB, Martin GR and Grahn D. Decreased lysyl oxidase activity in the aneurysm-prone, mottled mouse. *J Biol Chem*. 1977;252:939-42.
61. Thomas M, Gavrila D, McCormick ML, Miller FJ, Jr., Daugherty A, Cassis LA, Dellsperger KC and Weintraub NL. Deletion of p47phox attenuates angiotensin II-induced abdominal aortic aneurysm formation in apolipoprotein E-deficient mice. *Circulation*. 2006;114:404-413.
62. Chen GF, Sudhahar V, Youn SW, Das A, Cho J, Kamiya T, Urao N, McKinney RD, Surenkhuu B, Hamakubo T, Iwanari H, Li S, Christman JW, Shantikumar S, Angelini GD, Emanueli C, Ushio-Fukai M and Fukai T. Copper Transport Protein Antioxidant-1 Promotes Inflammatory Neovascularization via Chaperone and Transcription Factor Function. *Sci Rep*. 2015;5:14780.
63. Schmalz G, Schuster U and Schweikl H. Influence of metals on IL-6 release in vitro. *Biomaterials*. 1998;19:1689-94.
64. Suska F, Esposito M, Gretzer C, Kalltorp M, Tengvall P and Thomsen P. IL-1alpha, IL-1beta and TNF-alpha secretion during in vivo/ex vivo cellular interactions with titanium and copper. *Biomaterials*. 2003;24:461-8.
65. Cheuk BL and Cheng SW. Identification and characterization of microRNAs in vascular smooth muscle cells from patients with abdominal aortic aneurysms. *J Vasc Surg*. 2014;59:202-9.

Highlights

- Cu chelator markedly inhibited angiotensin II (Ang II)-induced abdominal aortic aneurysm (AAA).
- Human and mouse AAA tissues showed decreased Cu exporter ATP7A expression compared to non-AAA tissues.
- ATP7A dysfunctional mutant mice exhibited robust AAA formation and increased aortic Cu accumulation, vascular inflammation, and vascular smooth muscle cell loss.
- Mechanistically, miR125b, which targets anti-inflammatory Suv39h1 and TNFAIP3, was highly upregulated in AAA from ATP7A dysfunctional mutant mice in a Cu-dependent manner.
- LNA-modified anti-miR125b prevented vascular inflammation and AAA development in Ang II-infused or ATP7A dysfunctional mice.
- Cu chelation therapy or enhancing Cu transporting function of ATP7A that limits miR-125b may be potential therapeutic approach for treating inflammatory vascular disease.

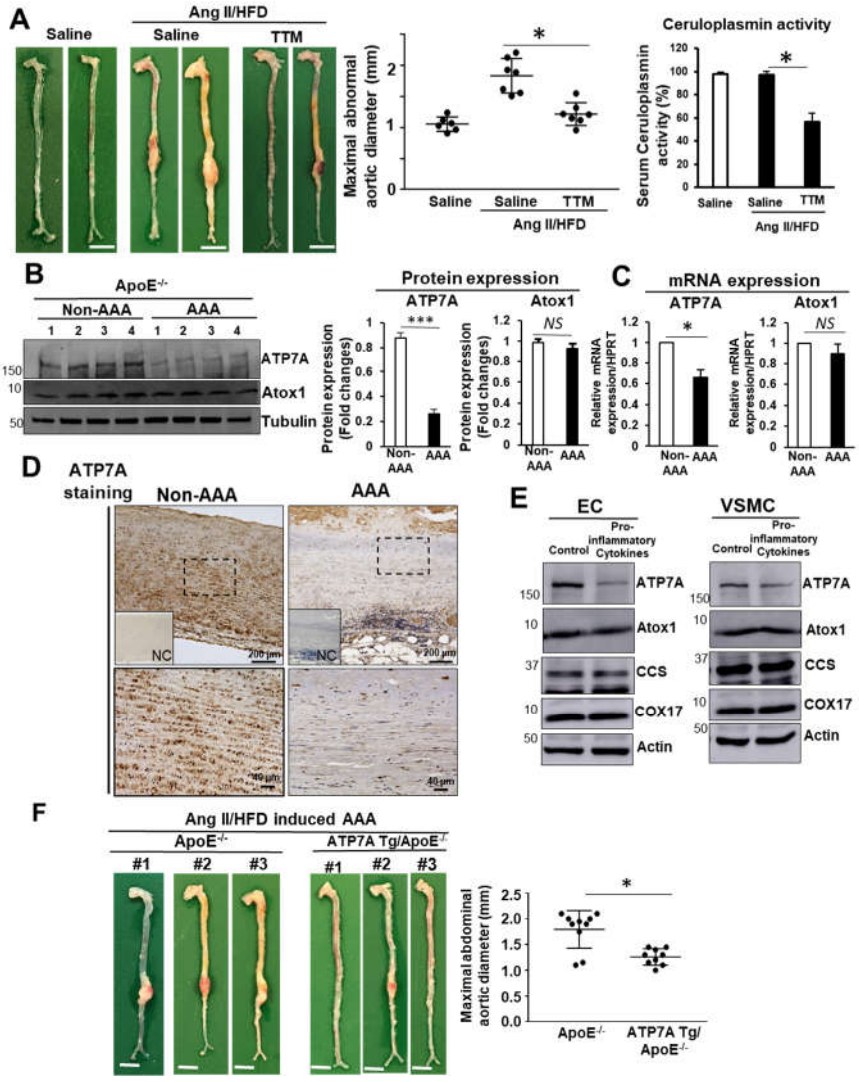

Figure 1. ATP7A expression is reduced in Ang II-induced AAA, while ATP7A overexpression or administration of a Cu chelator prevents Ang II-induced AAA formation in ApoE$^{-/-}$ mice. (A, B, C) ApoE$^{-/-}$ mice were infused with Ang II on a HFD or saline for 4 weeks with or without Cu chelator TTM. **A,** Representative images of whole aorta (left). Scale bars: 3 mm. Maximal abdominal aortic diameter (middle panel) and serum ceruloplasmin activity in aorta (right). (n=4). **B,** Western blot of ATP7A and Atox1 proteins in mouse abdominal aorta tissues (n=8). **C,** Quantitative real-time PCR analysis of ATP7A or Atox1 mRNA expression in abdominal aorta (n=4). **D**, Immunohistochemical staining of ATP7A in human AAA and non-AAA tissue (n=3 for AA or N=3 for non-AA). *Inset*, absence of staining when mouse IgG was used as antibody isotype negative controls (NC). High magnification of region within rectangle are shown at lower panel. **E**, ECs from bovine aorta (BAEC) and VSMC from rat aorta (RASM) were incubated with pro-inflammatory cytokine cocktail (TNFα (10 ng/ml), IL-1β (10 ng/ml) and IL-6 (10 ng/ml) for 24 hrs and then used to measure protein expression. (n=4). Quantifications were showed in Supplementary figure II. **F,** Representative images of whole aorta from ApoE$^{-/-}$ or ATP7A Tg/ApoE$^{-/-}$ mice following 4 weeks Ang II infusion with HFD. Scale bars: 3 mm. Maximal abdominal aortic diameter (right panel, n=9). *p<0.05.

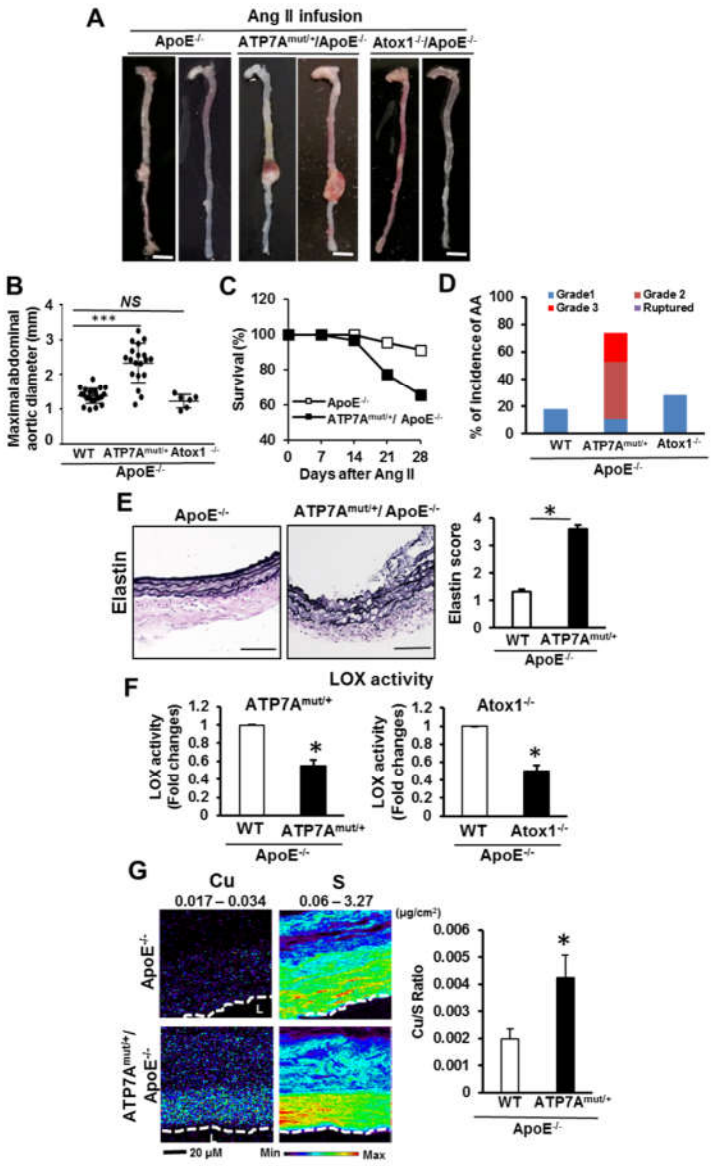

Figure 2. ATP7A dysfunction, but not lack of Atox1, augments AAA formation. (**A-F**) ApoE$^{-/-}$, ATP7A$^{mut/+}$/ApoE$^{-/-}$ or Atox1$^{-/-}$/ApoE$^{-/-}$ mice following 4 weeks of Ang II infusion without HFD were examined. **A,** Representative images of whole aorta. Scale bars: 3 mm. **B and C**, Maximal abdominal aortic diameter (B), Kaplan–Meier curves of survival (C) in ApoE$^{-/-}$ (n=23), ATP7A$^{mut/+}$/ApoE$^{-/-}$ (n=19) and Atox1$^{-/-}$/ApoE$^{-/-}$ (n=6) mice. **D,** Incidence and severity of AA. See the Online Methods for grading aneurysm severity. **E,** Representative images of elastin integrity of abdominal aortic sections from ApoE$^{-/-}$ (n=23) and ATP7A$^{mut/+}$/ApoE$^{-/-}$ (n=21) mice and quantitative analysis of grading for elastin degradation. Scale bars: 20 μm. **F**, LOX activity in aortic tissue. n=4. **G**, Aortic Cu content in ApoE$^{-/-}$ or ATP7A$^{mut/+}$/ApoE$^{-/-}$ mice following 4 weeks of Ang II infusion as measured by synchrotron-based x-ray fluorescence (XFM). XFM scans (1–2 seconds per pixel) were performed in paraffin-embedded tissues. The maximum and minimum threshold values in microgram per square centimeter are given above each frame. Map of Cu shows areas of the lowest to the highest content scaled to a rainbow color (bottom). Total sulfur is used as a surrogate for total cellular protein and to visualize the morphology of tissue sections. n=5. *p<0.05, ***p<0.001.

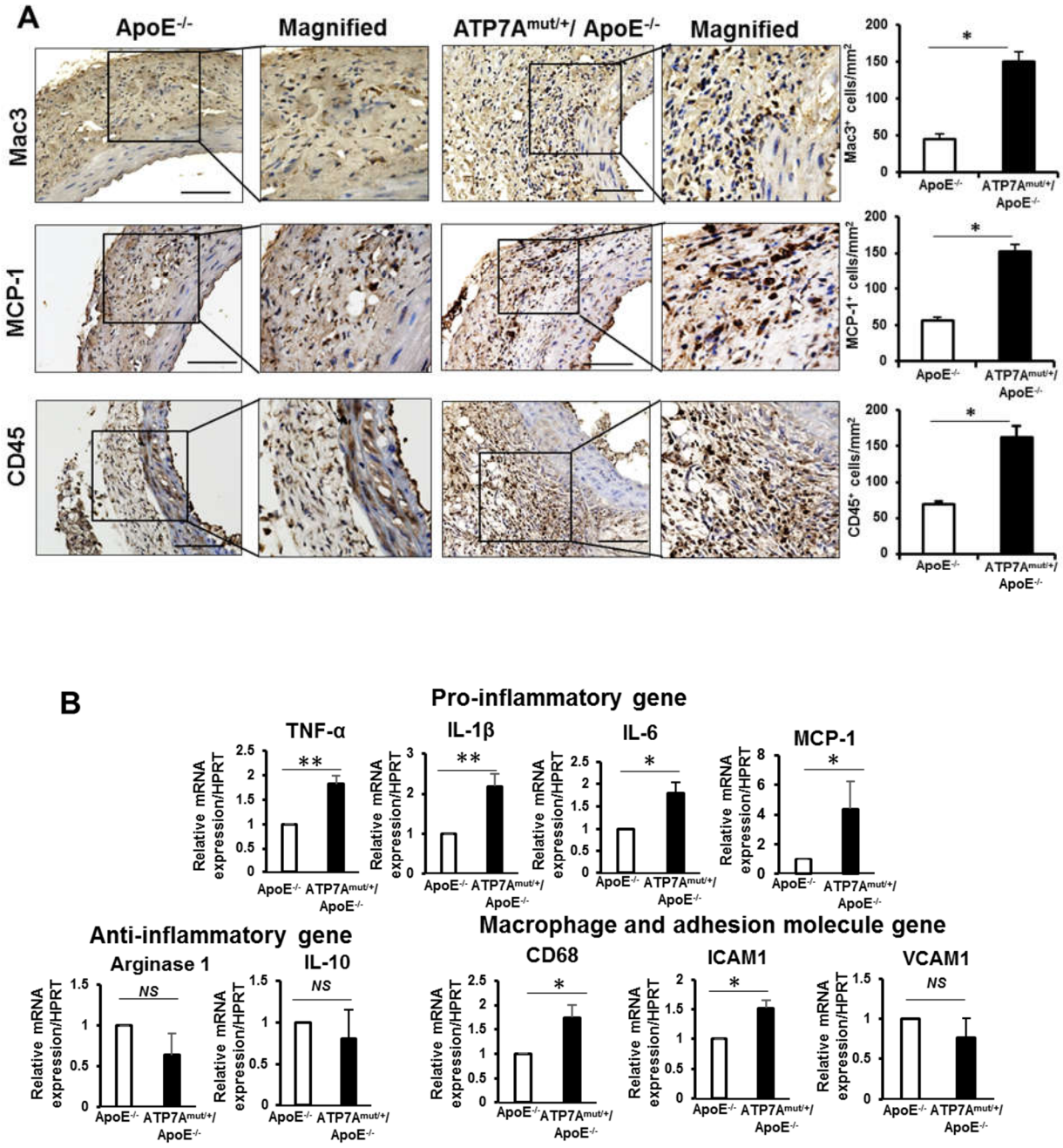

Figure 3. ATP7A dysfunction promotes proinflammatory responses in AAA. (A and B) Abdominal aorta tissues from ApoE$^{-/-}$ and ATP7A$^{mut/+}$/ApoE$^{-/-}$ mice following 4 weeks of Ang II infusion were examined. **A,** Representative images of immunohistochemical staining for macrophages (Mac3) and Monocytes chemoattractant protein-1 (MCP-1) and quantification. **B**, Dynamic expression profiles of inflammatory genes expression measured by qPCR (n=4). *p<0.05.

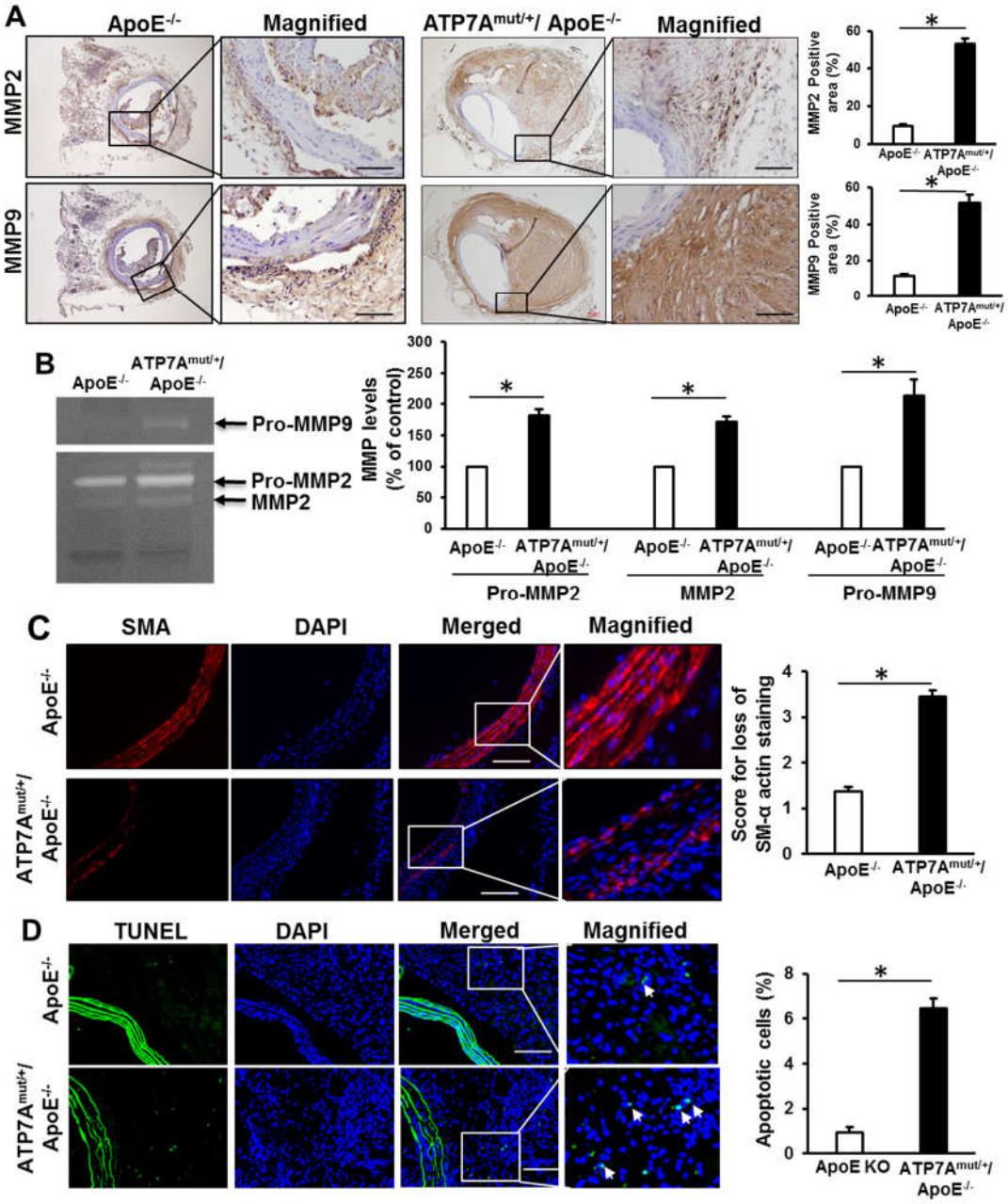

Figure 4. ATP7A dysfunction promotes MMP expression, apoptosis and loss of VSMCs in aortas following 4 weeks of Ang II infusion. (A-D) Abdominal aorta tissues from ApoE$^{-/-}$ and ATP7A$^{mut/+}$/ApoE$^{-/-}$ mice following 4 weeks of Ang II infusion were examined. **A**, Immunohistochemical staining for MMP2 and MMP9 and quantification (n=7-11). **B,** Representative zymogram (top) and quantified data (bottom) of MMP levels in aorta homogenates (n=4). **C,** Immunofluorescence staining for SMC loss assessed by SMA staining and quantification (n=11). Score 1, intact media, no SMC loss; score 2, modest loss of SMC; score 3, severe loss of SMC; score 4, rupture of media, almost no SMC left. **D**, Immunofluorescence staining of apoptotic cells using TUNEL staining and quantification (n=10). Scale bars: 20 μm. *p<0.05.

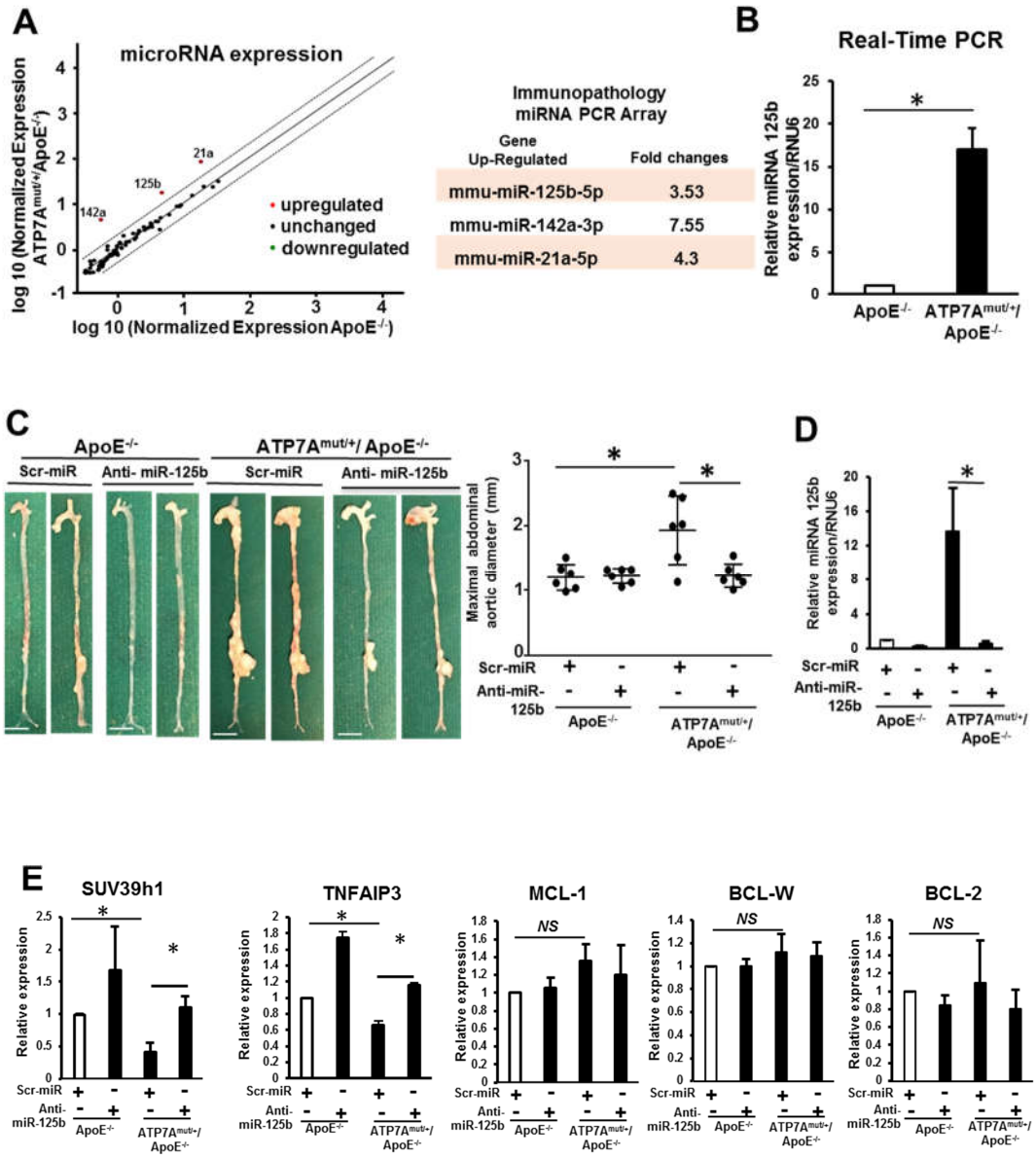

Figure 5. Anti-miRNA 125b treatment abolishes the development of Ang II-induced AA formation in ATP7A$^{mut/+}$/ApoE$^{-/-}$ mice. Abdominal aorta tissues from ApoE$^{-/-}$ and ATP7A$^{mut/+}$/ApoE$^{-/-}$ mice following 4 weeks of saline or Ang II infusion were examined. (**A)** Identification of aortic miRNAs in ApoE$^{-/-}$ or ATP7A$^{mut/+}$/ApoE$^{-/-}$ mice infused with Ang II for 4 weeks using the Qiagen miScript miRNA. Immunopathology array (n=3/group) and miScript PCR Array Data Analysis Tool. (**B**) miRNA 125b was validated using Real time-qPCR (n=4). (**C,D,E**) Representative images and maximum diameter of aorta (**C**), quantification of miRNA 125b expression (n=4) (**D**), andmiR-125b target gene expression analysis (n=4) using real-time qPCR (**E**) of mice with or without intravenous injection of LNA modified Anti-miRNA 125b or scrambled control. In **C**, scale bars: 3 mm. Maximal abdominal aortic diameter (Middle) with or without anti-miRNA 125b treatment (n=4). *p<0.05.

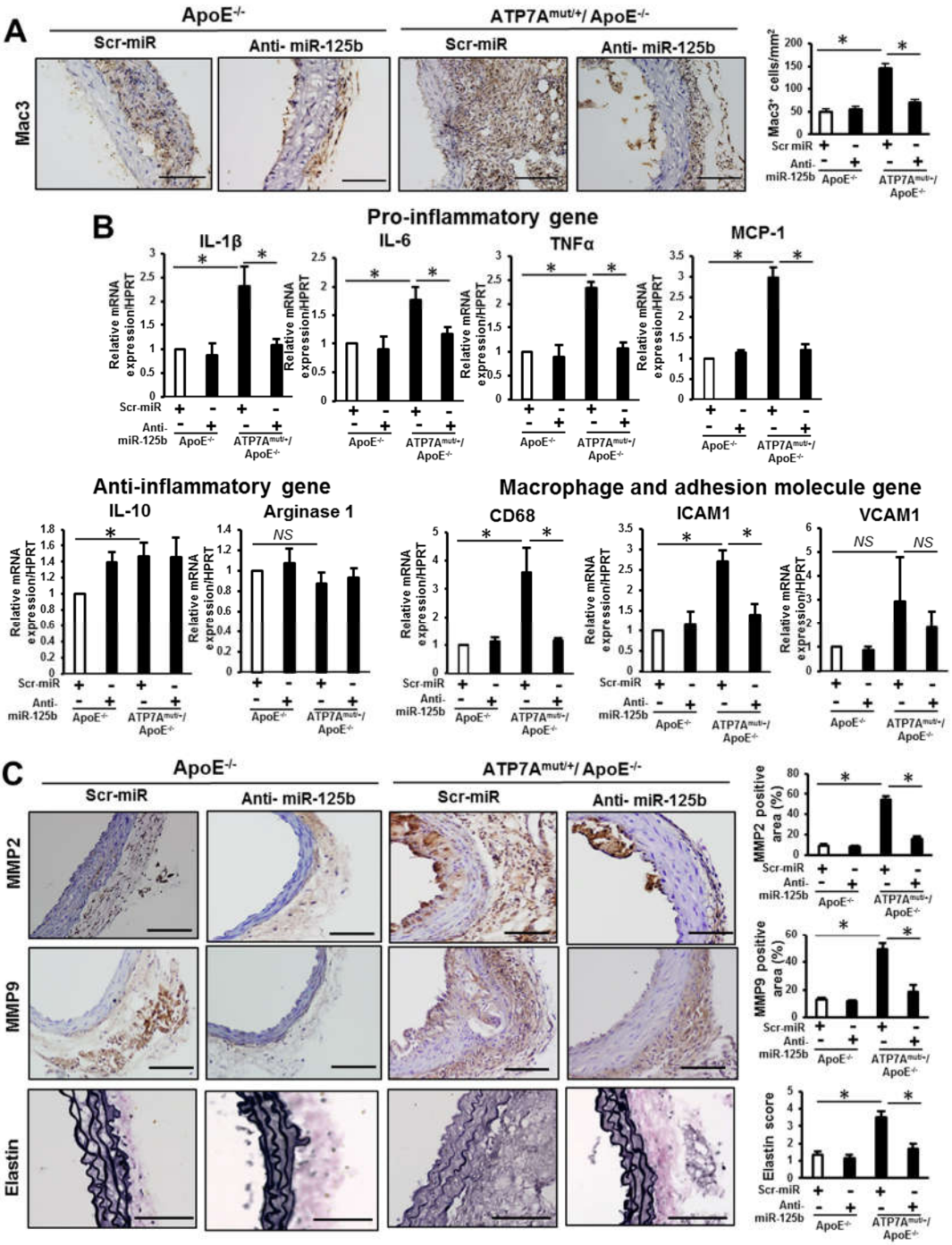

Figure 6. Anti-miRNA 125b decreased Mac3 expression, MMP expression, apoptosis and loss of SMCs in aorta from Ang II-infused ATP7A$^{mut/+}$/ApoE$^{-/-}$ mice. Abdominal aorta tissues from ApoE$^{-/-}$ or ATP7A$^{mut/+}$/ApoE$^{-/-}$ mice following 4 weeks of Ang II infusion with or without anti-miRNA 125b treatment were examined. **A,** Representative images of immunohistochemical staining for macrophages (Mac3) and quantification (n=4). Scale bars: 20 μm. **B**, Expression profiles of inflammatory genes by real-time qPCR (n=4). **C**, Immunohistochemical staining for MMP2 (top) and MMP9 (middle) and representative images of elastin integrity (bottom) and quantification (right) (n=4).

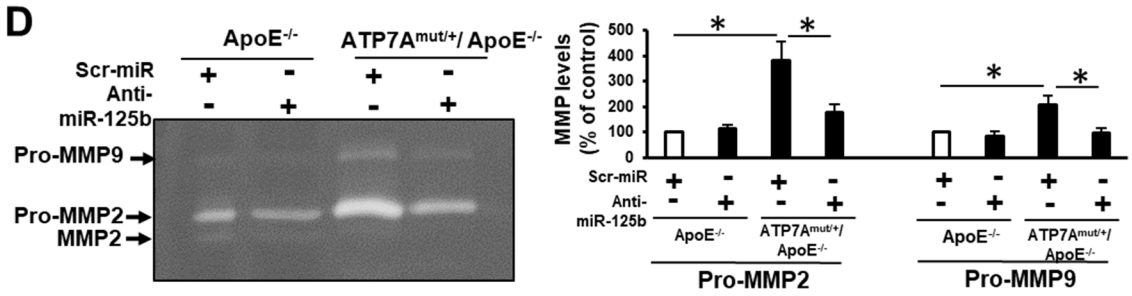

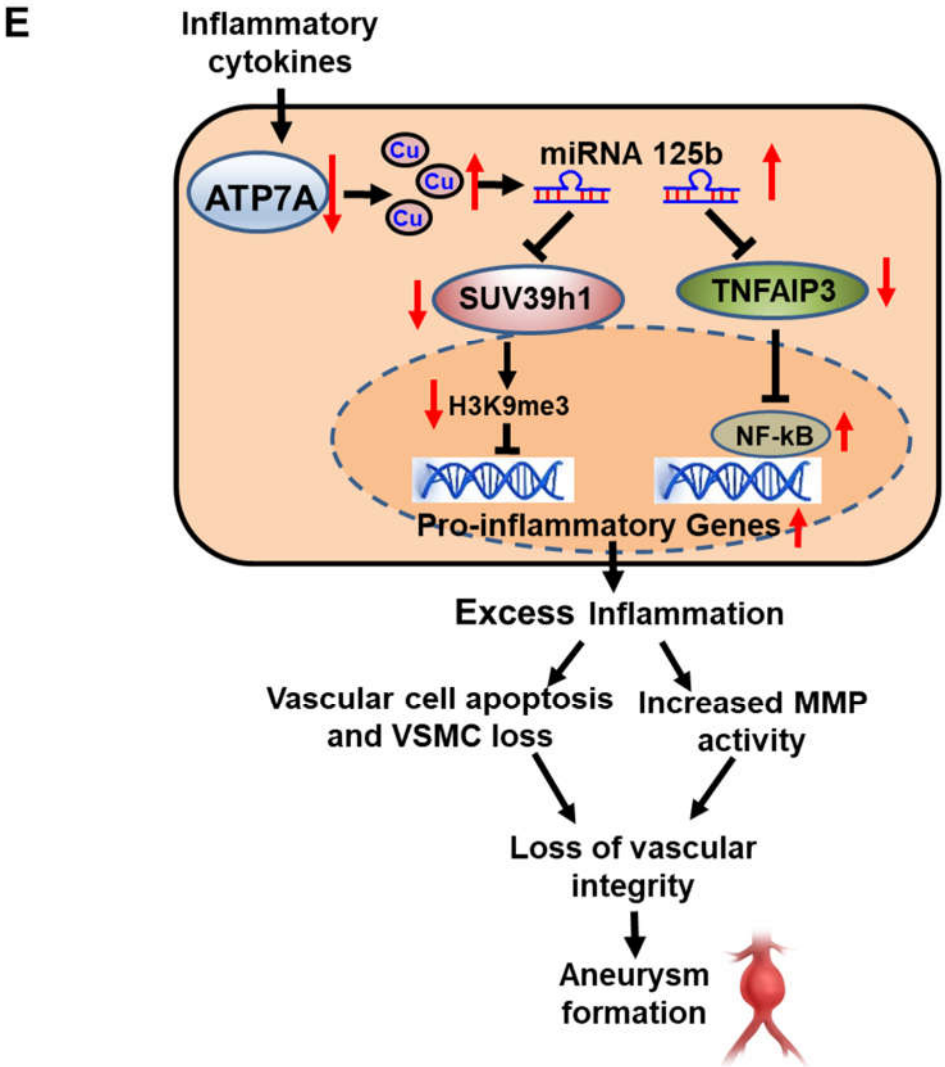

D, Representative zymogram (top) of pro-MMP-2 and pro-MMP-9 levels and quantification (right). Scale bars: 20 μm. *p<0.05. **E, Proposed model for the protective role of ATP7A against inflammation and smooth muscle cell apoptosis in experimental aortic aneurysm.** ATP7A downregulation promotes AA formation by increasing vascular inflammation, in part via inducing miR-125b, thereby increasing MMP activity, elastin fragmentation, vascular apoptosis, and VSMC loss,. Thus, ATP7A is a potential therapeutic target for inflammatory vascular disease.

SUPPLEMENTARY FIGURES

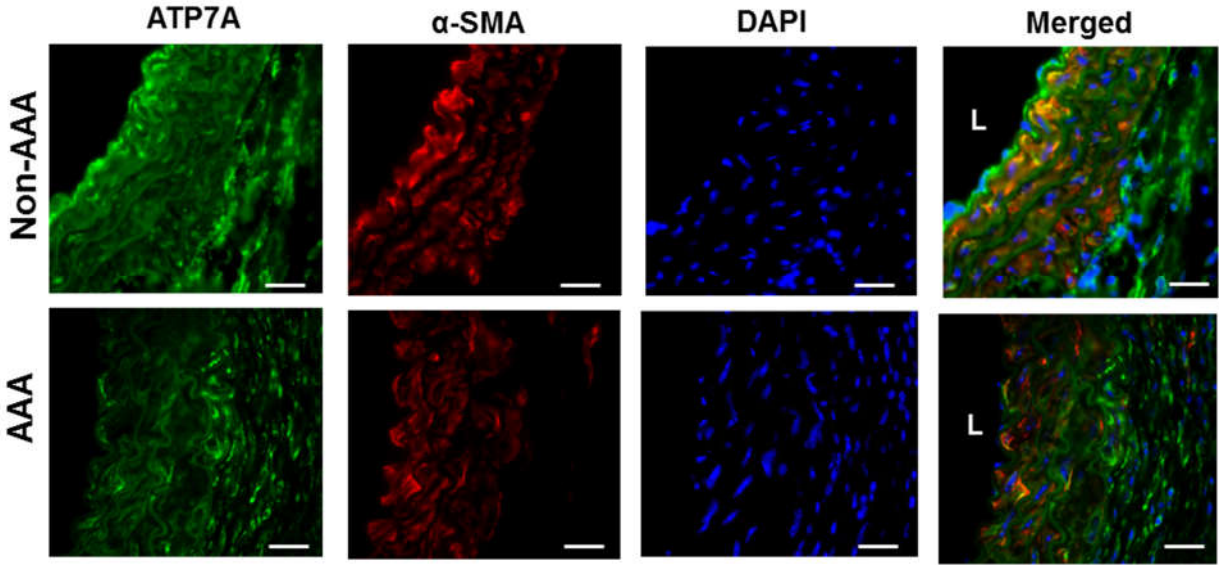

Supplementary Figure I. ATP7A expression is reduced in Ang II/HFD induced AAA. Representative immunofluorescence image of ATP7A in smooth muscle cells of AAA or non AAA aorta from ApoE$^{-/-}$ mice infused with Ang II on HFD or saline for 4 weeks, respectively, using anti-ATP7A (green) and α-smooth muscle actin (red) antibodies. Scale bar 10 μm.

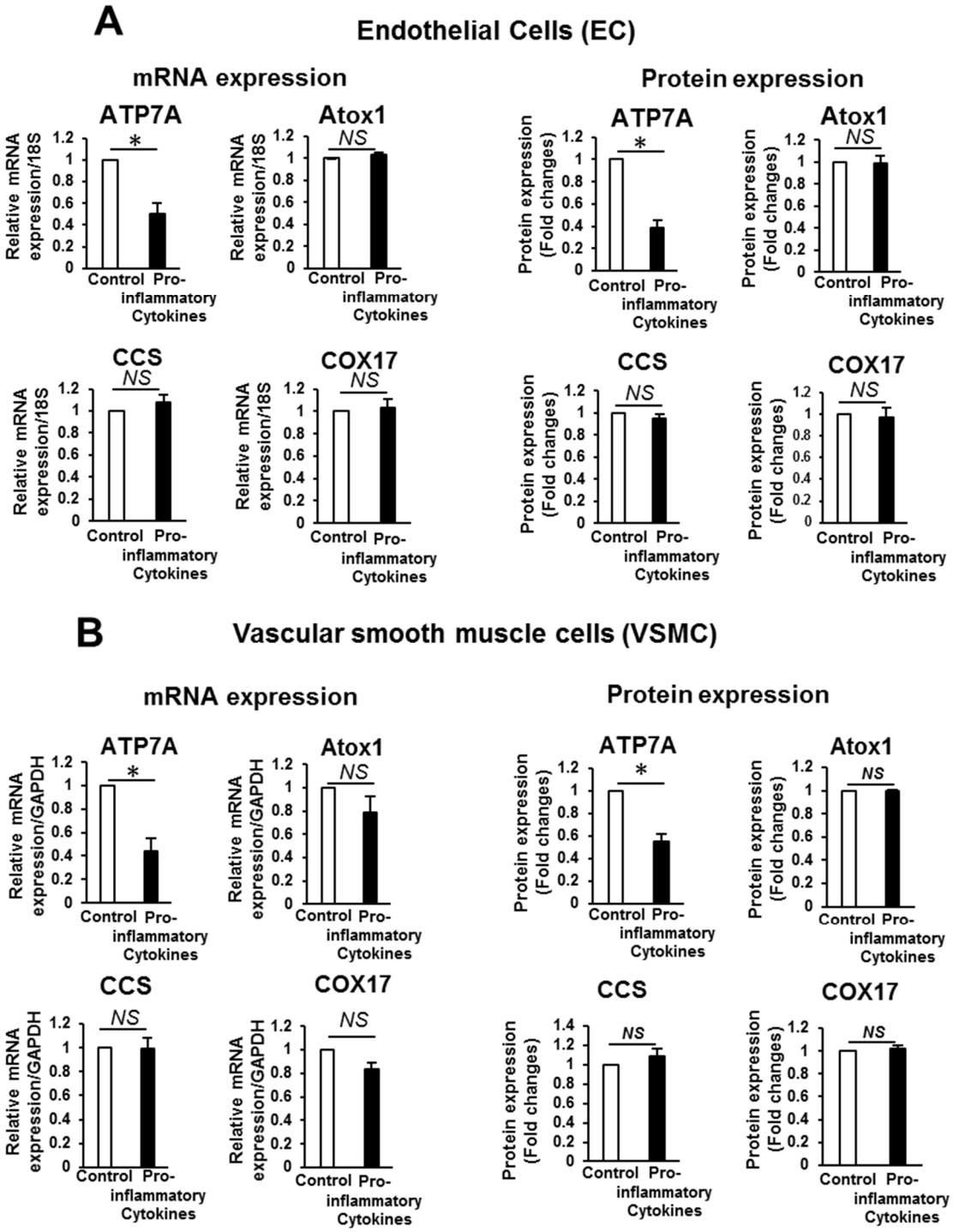

Supplementary Figure II. ATP7A mRNA and protein expressions are decreased by pro-inflammatory cytokines cocktail in endothelial cells (EC) and Vascular smooth muscle cells (VSMC). ECs from bovine aorta (A) and VSMC from rat aorta (B) were incubated with pro-inflamamtory cytokine cocktail (TNFα (10 ng/ml), IL-1β (10 ng/ml) and IL-6 (10 ng/ml) for 24 hrs and then used to measure mRNA (left) and protein (right) expression using real-time PCR and western blot respectively. N=4. *$p<0.05$. NS, not significant

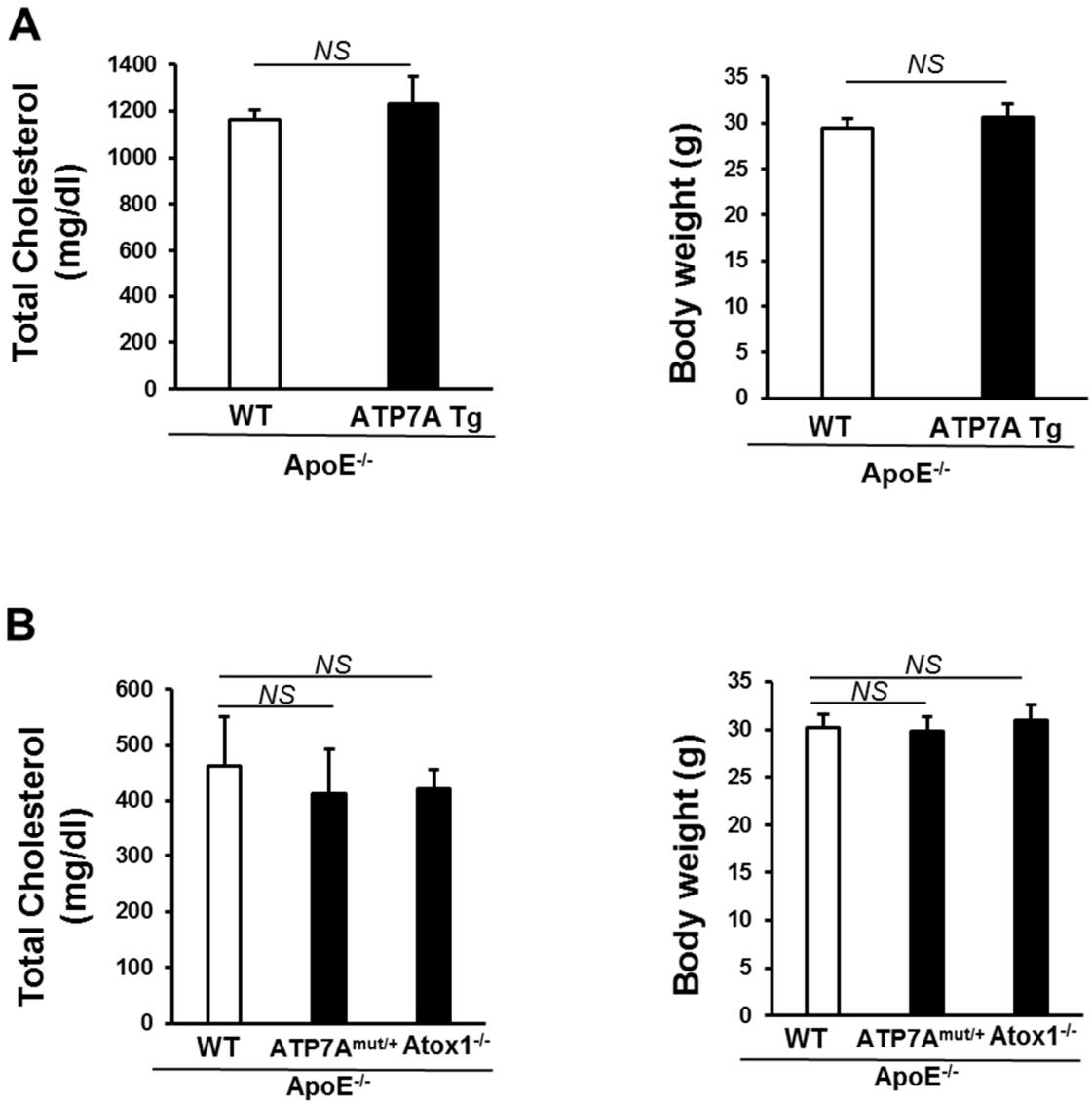

Supplementary Figure III. There was no significant difference in Cholesterol level and Body weight among ApoE$^{-/-}$or ATP7A$^{mut/+}$/ApoE$^{-/-}$ or Atox1$^{-/-}$/ApoE$^{-/-}$ mice. Plasma cholesterol levels (left panel) were measured in mice after overnightfasting according to manufacturer instructions as showed in method section and measure Body weight (right panel)) in Ang II/HFD-treated (A) and Ang II-infused (B) mice. n= 6-10 mice in each group. Results are presented as mean ± SEM. NS, not significant.

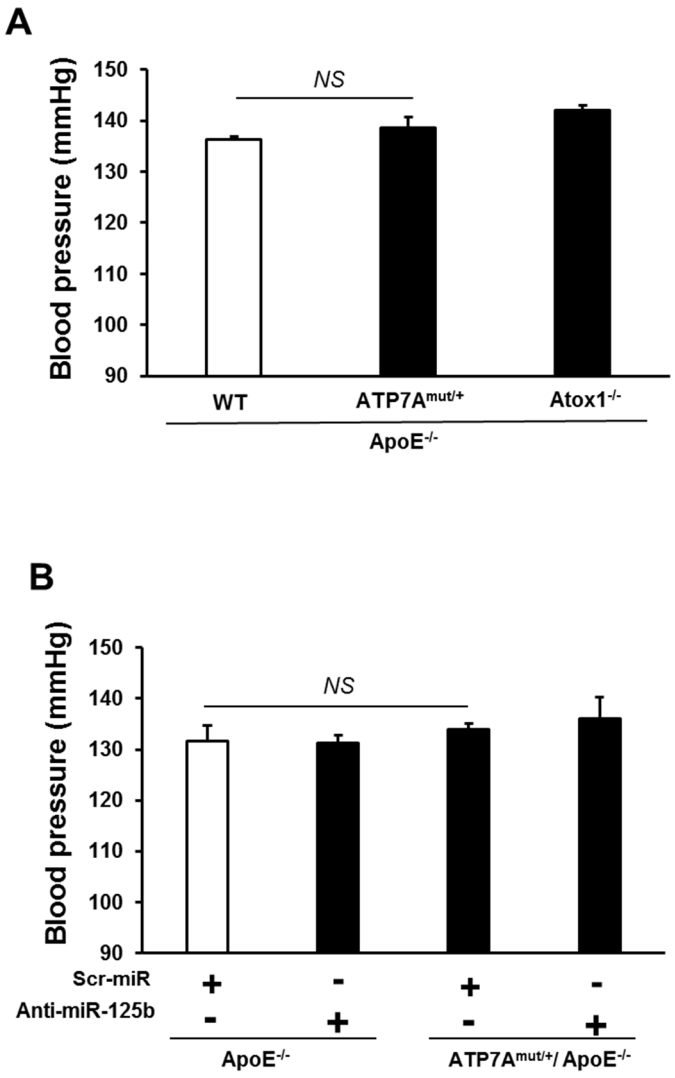

Supplementary Figure IV. There was no significant difference in blood pressure among Ang–II infused ApoE$^{-/-}$or ATP7A$^{mut/+}$/ApoE$^{-/-}$ or Atox1$^{-/-}$/ApoE$^{-/-}$ mice. (A-B) Blood pressure was measured in ApoE$^{-/-}$ or ATP7A$^{mut/+}$/ApoE$^{-/-}$ or Atox1$^{-/-}$/ApoE$^{-/-}$ mice (**A**) after AngII infusion with or without Anti-miRNA treatment (**B**). N=5-6 in each group. NS, not significant.

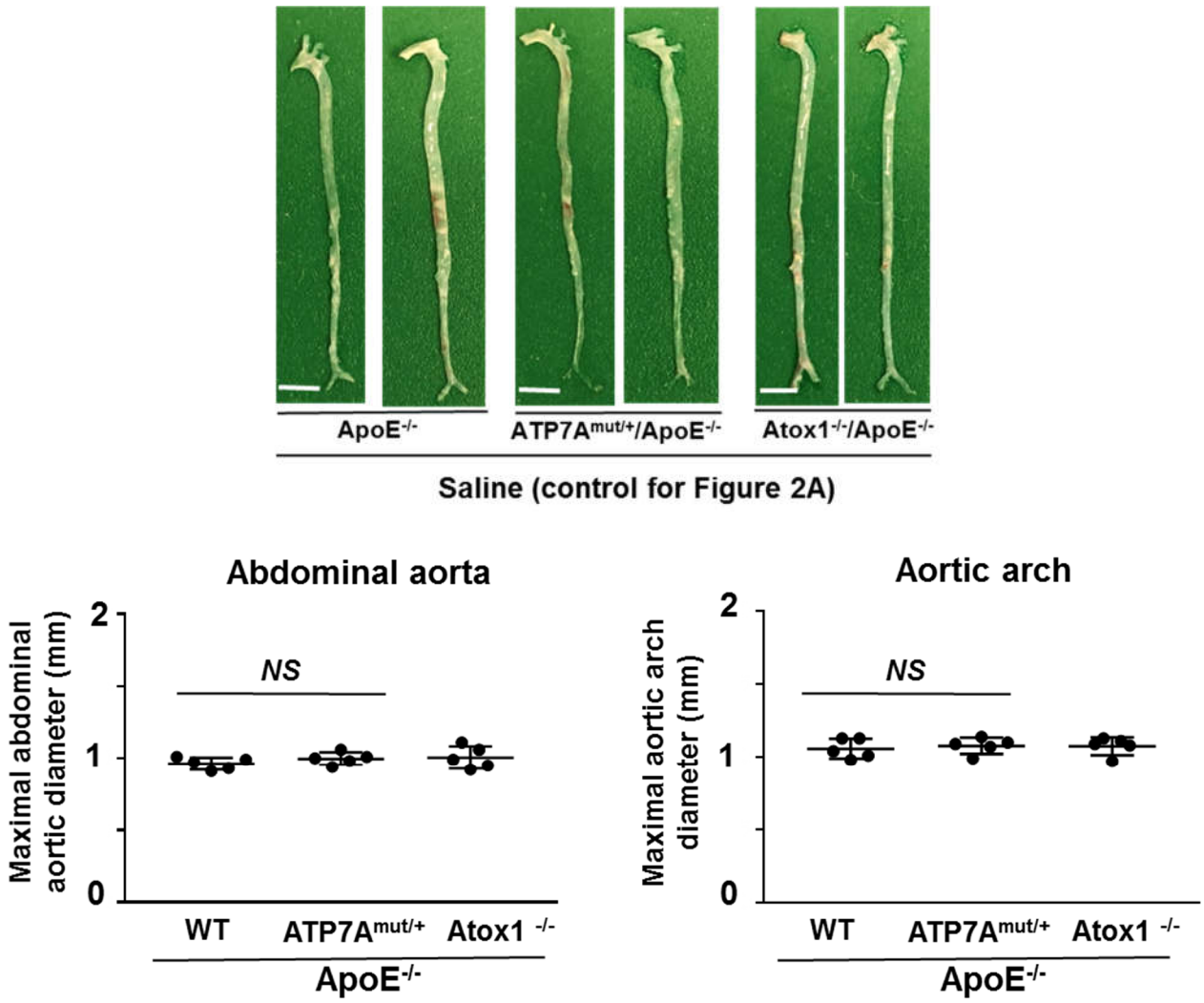

Supplementary Figure V. Both ATP7A$^{mut/+}$/ApoE$^{-/-}$ mice and Atox1$^{-/-}$/ApoE$^{-/-}$ mice with saline infusion do not show aortic aneurysm formation. Representative image of whole aorta. Saline (vehicle for AngII) were infused in each mice at 3-4 month old in a similar fashion as Figure 2A (i.e. Age-matched control with Figure 2A). bottom, Maximal abdominal aortic or aortic arch diameter in these mice. Scale bars: 3 mm.

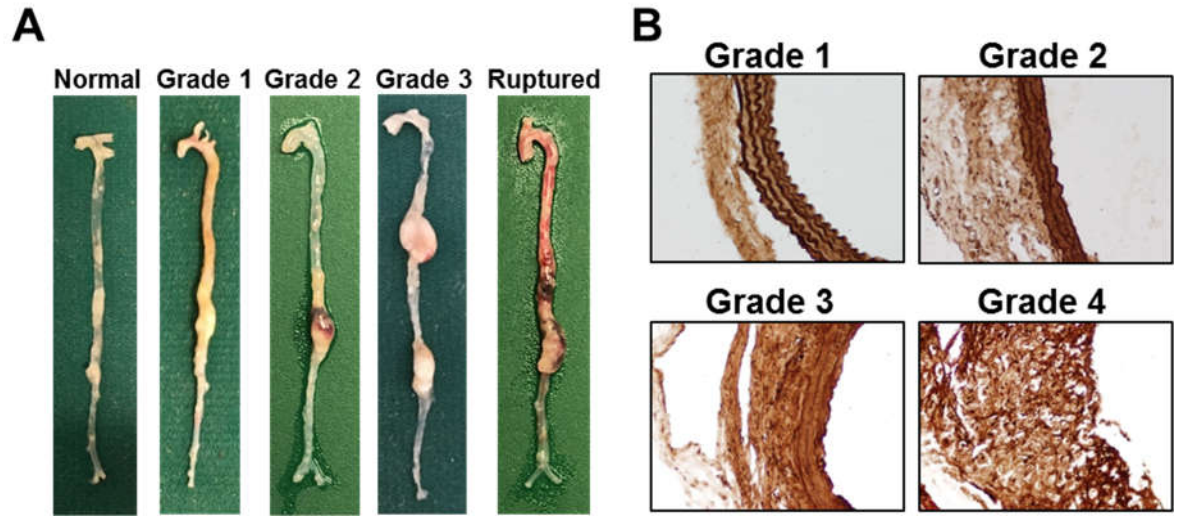

Supplemental figure VI. A, Aneurysm severity was graded according to the following criteria: Grade 1, remodeled tissue in the suprarenal region with pronounced bulbous; Grade 2, pronounced bulbous form of grade 1 containing thrombus; Grade 3, multiple aneurysms containing thrombus; or ruptured, ruptured aortic aneurysm, **B,** Elastin grading criteria. Grade 1, intact elastic laminae; Grade 2, elastic laminae with interruptions and breaks; Grade 3, severe elastin fragmentation; and Grade 4, severe elastin digestion with visible ruptured sites.

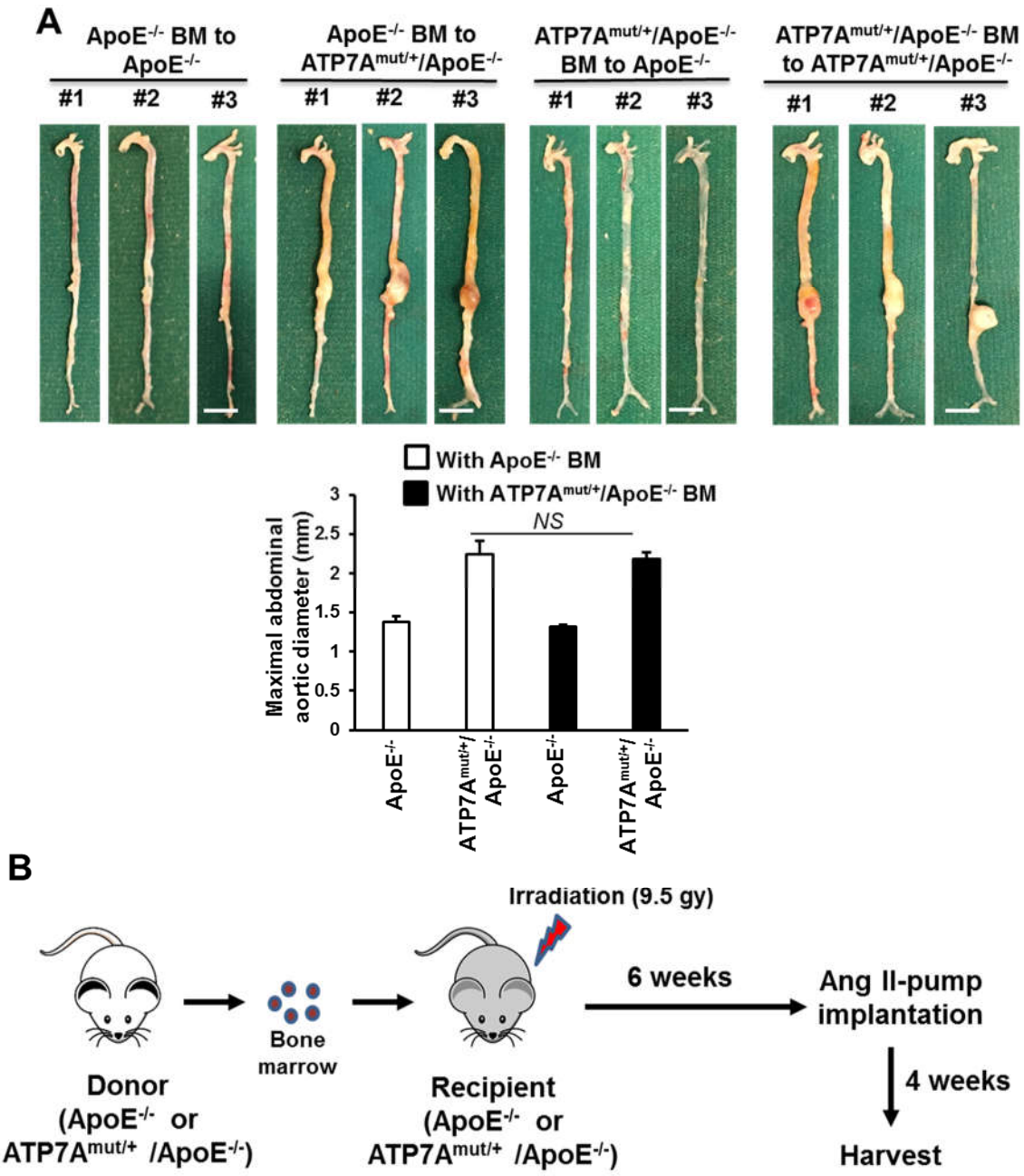

Supplementary Figure VII. AAA phenotype in ATP7A$^{mut/+}$mice is intrinsic to the vascular wall. (A) Representative image of whole aorta of bone marrow (BM) transplanted mice following Ang-II infusion (N=5 in each group), Scale bar 3 mm. bottom, Maximal abdominal aortic diameter in these mice. NS, not significant. **(B)** Schematic representation of bone marrow transplantation experiment.

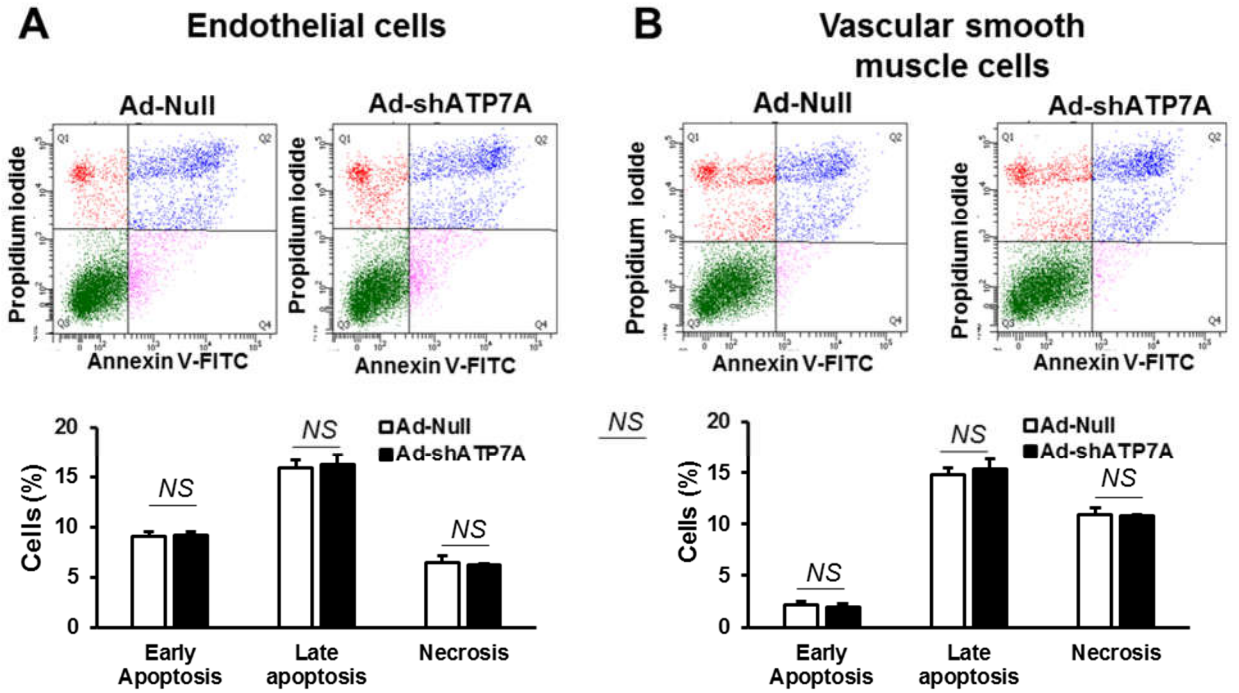

Supplementary Figure VIII. ATP7A knockdown per se did not induce apoptosis in vascular cells. Apoptosis was measured in human endothelial cells (HUVEC) and human aortic vascular smooth muscle cells (HASM) after knockdown of ATP7A using adeno-shATP7A for 48 hrs by flow cytometry using annexin V-FITC/PI staining. **Top**, representative flow cytometry dot plots showing the percentage of cells in viable, early apoptotic, late apoptotic and necrotic stages in endothelial cells (**A**) or Vascular smooth muscle cells (**B**). **Bottom**, quantification of the cell viability. Data are presented as the mean ± SEM. NS, not significant.

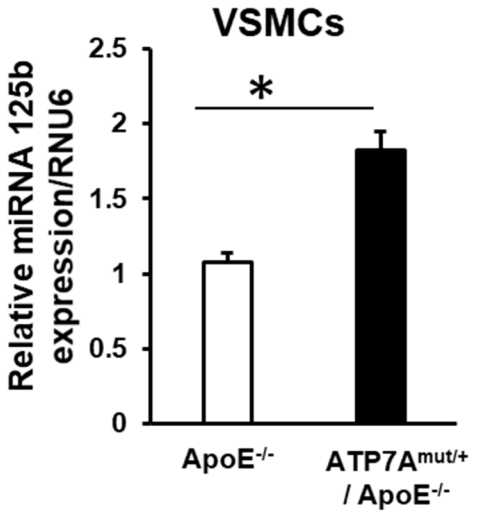

Supplementary Figure IX. **miRNA 125b expression is increased in vascular smooth muscle cells isolated from ATP7A$^{mut/+}$/ApoE$^{-/-}$ mice with AngII infusion**. Vascular smooth muscle cells (VSMCs) were isolated from aorta of ApoE $^{-/-}$ and ATP7A$^{mut/+}$/ApoE$^{-/-}$ mice infused with Ang II for 4 weeks and measured miRNA 125b using quantitative RT-PCR (N=3). Results are presented as mean ± SEM. *$p<0.05$.

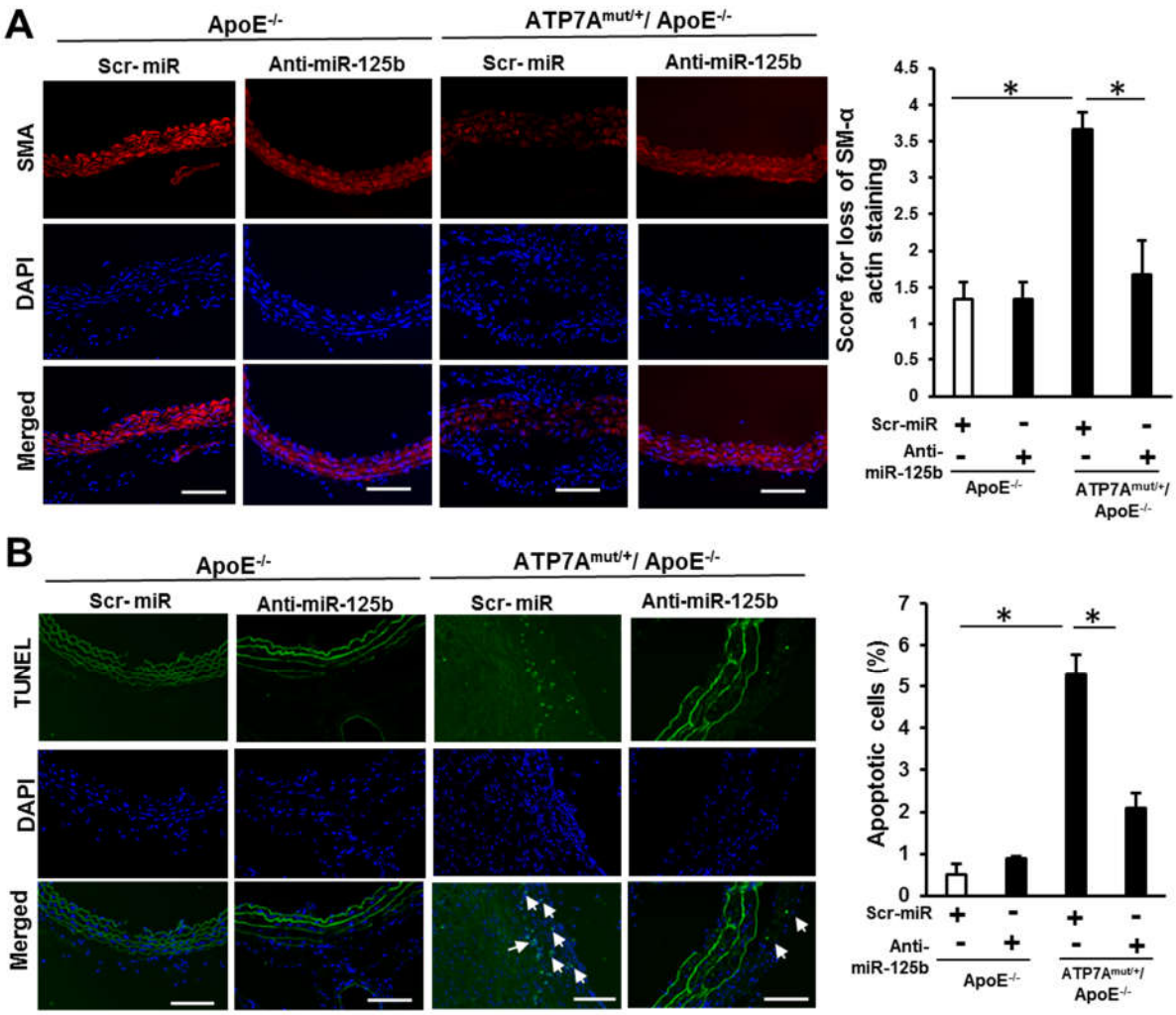

Supplementary Figure X. Anti-miRNA 125b decreased apoptosis and loss of SMCs in in aorta from Ang II infused ATP7A$^{mut/+}$/ApoE$^{-/-}$ mice. Immunofluorescence analysis in abdominal aorta tissue from ApoE$^{-/-}$ or ATP7A$^{mut/+}$/ApoE$^{-/-}$ mice following 4 weeks of Ang II infusion with or without anti-miRNA 125b treatment. **(A)** Immunofluorescence staining for SMC loss assessed by SMA staining in abdominal aorta tissue and quantification as shown in Figure 3. (**B**) Immunofluorescence staining of apoptotic cells using TUNEL in abdominal aorta tissue and quantification in right panel (N=3). Scale bars: 20 μm. Results are presented as mean ± SEM. *p<0.05.

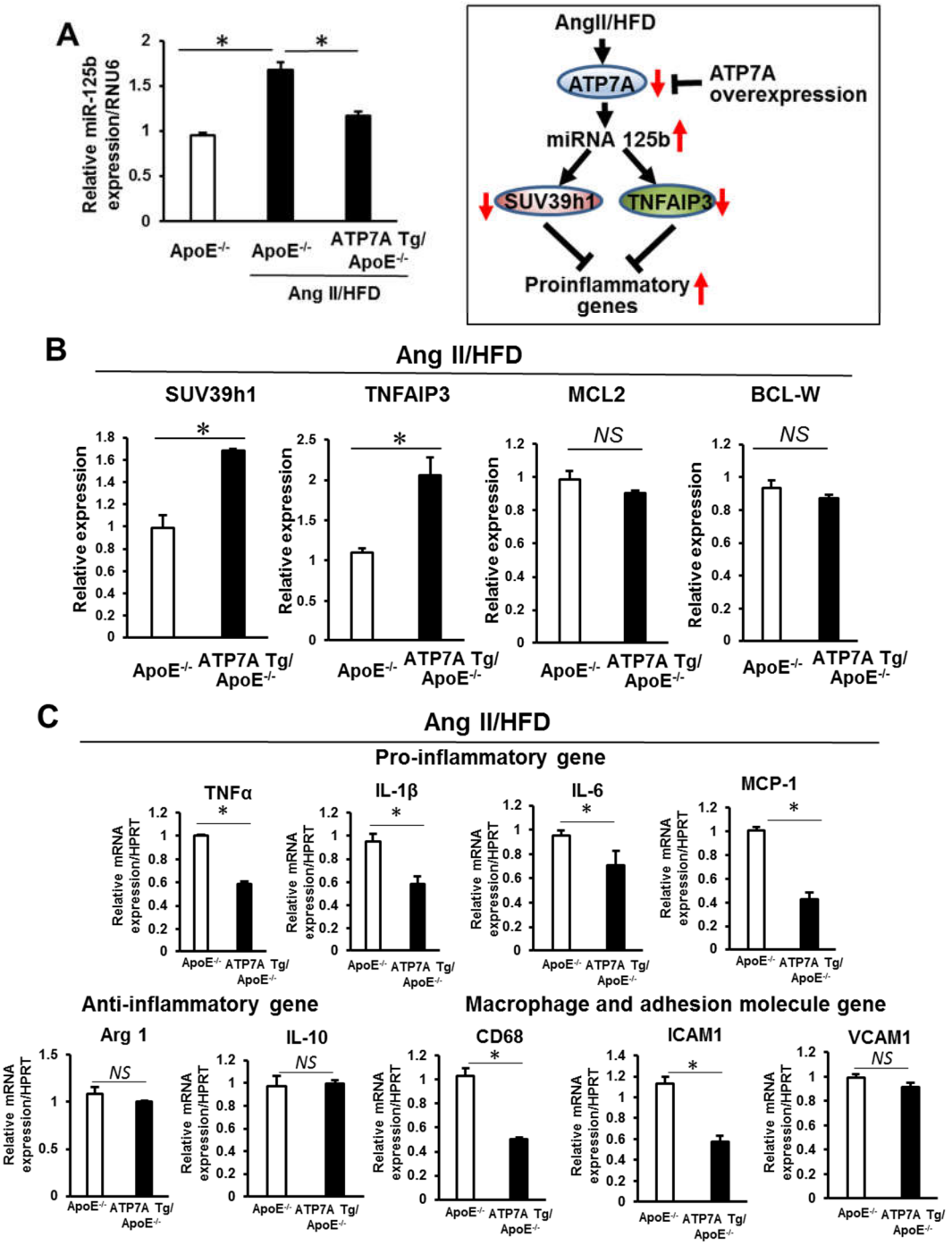

Supplementary Figure XI. Effect of ATP7A overexpression on miR-125b, miR-125b target gene expression and pro-inflammatory gene expression in Ang II/HFD-induced AAA. Abdominal aorta tissues were from ApoE$^{-/-}$ and ATP7A Tg/ApoE$^{-/-}$ mice infused with Ang II on HFD or saline for 4 weeks. Quantification of miR-125b expression (**A**) and miR-125b target gene (**B**) expression (SUV39h1, TNFAIP3, MCL2 and BCL-W) in aorta of mice (n=3) using real-time qPCR. **(C)** Dynamic expression profiles of inflammatory genes expression by real-time PCR (N=4). *p<0.05. NS, not significant. Results are presented as mean ± SEM. *p<0.05. NS, not significant.

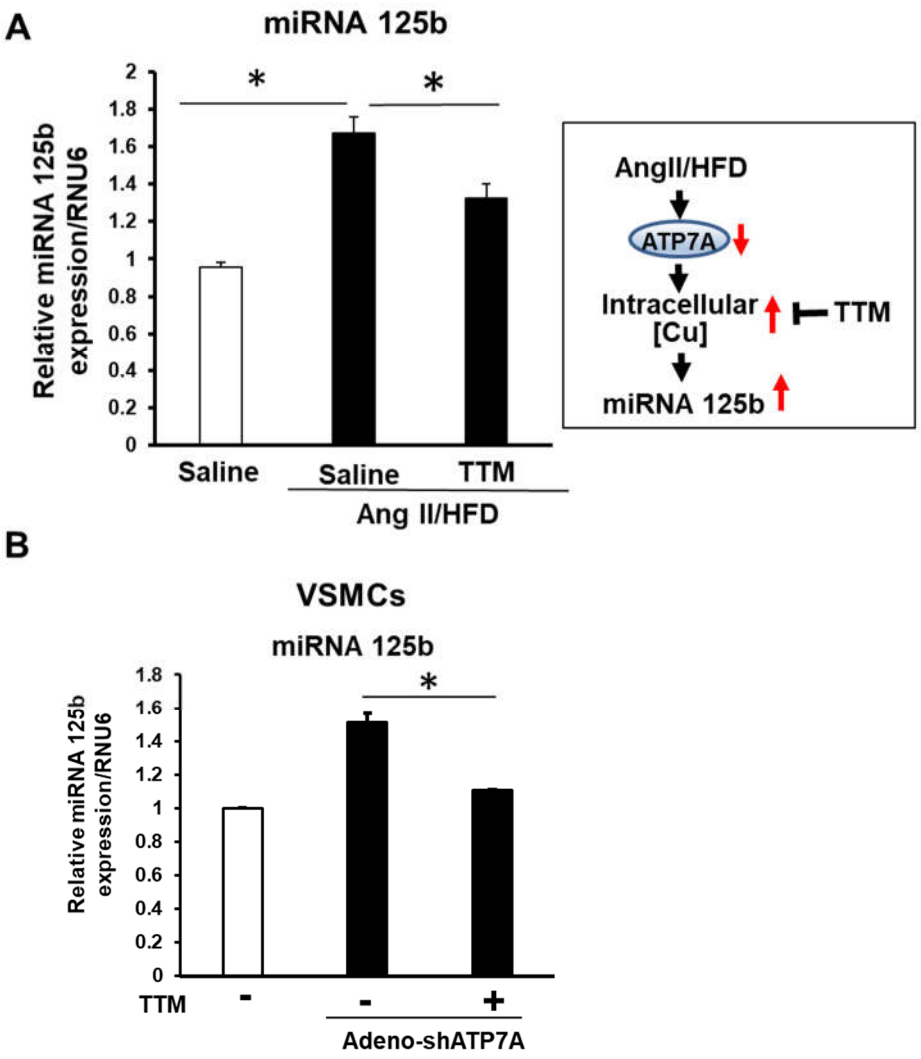

Supplementary Figure XII. A, TTM treatment prevented miRNA 125b upregulation in Ang II/HFD-induced AAA tissue. Abdominal aorta tissues from ApoE$^{-/-}$ mice following 4 weeks of Ang II infusion on HFD or saline with or without Cu chelator TTM were examined. Quantification of miRNA 125b expression in aorta of mice (n=4) using real-time qPCR. **B, TTM treatment prevented miRNA 125b upregulation induced by ATP7A knockdown in cultured VSMCs.** miRNA 125b was measured in human aortic vascular smooth muscle cells (VSMCs) after knockdown of ATP7A using adeno-shATP7A for 48 hrs with or without Cu chelator, TTM (20nM, 24 hrs) using quantitative RT-PCR. (N=3). Results are presented as mean ± SEM. *p<0.05.

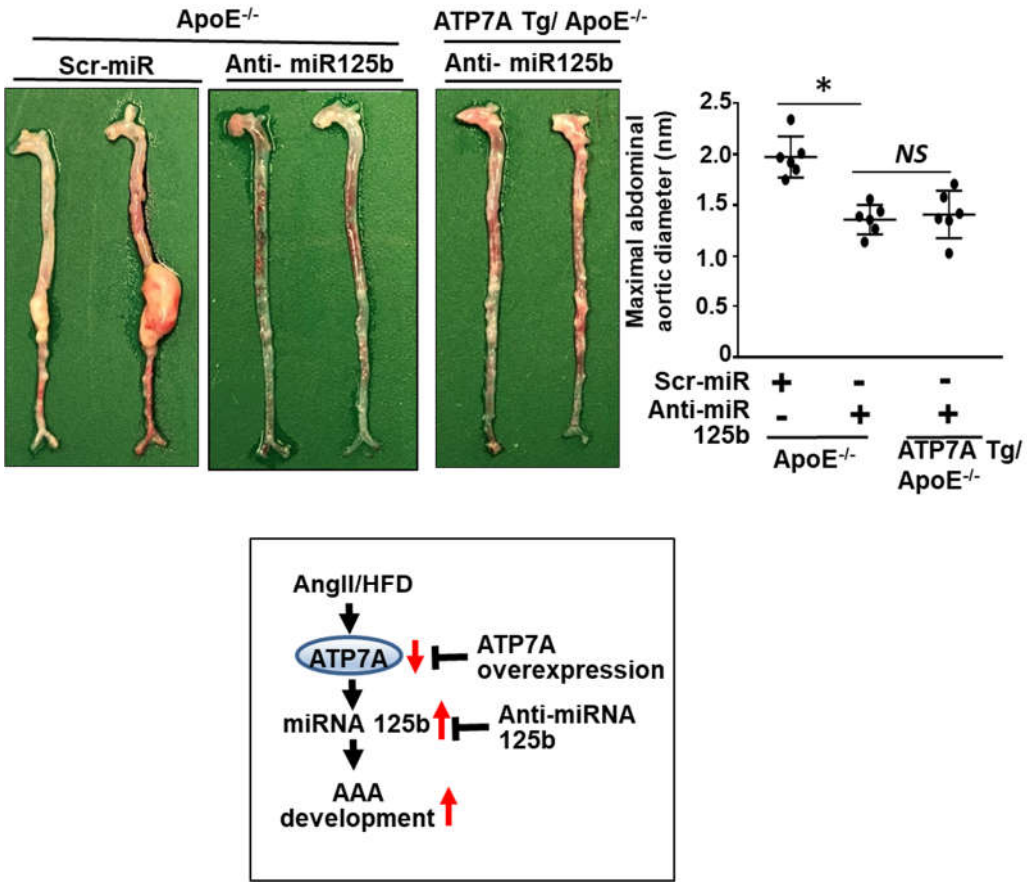

Supplementary Figure XIII. ATP7A overexpression has no additional preventive effects on anti-miR-125b-induced inhibitory effects on AAA formation. ApoE$^{-/-}$ or ATP7A Tg/ApoE$^{-/-}$ mice were infused with Ang II on HFD for 4 weeks with or without intravenous injection of LNA modified Anti-miRNA 125b or scrambled control. Left, representative images of whole aorta. Right, maximal abdominal aortic diameter (n=6). Results are presented as mean ± SEM. *p<0.05. NS, not significant.

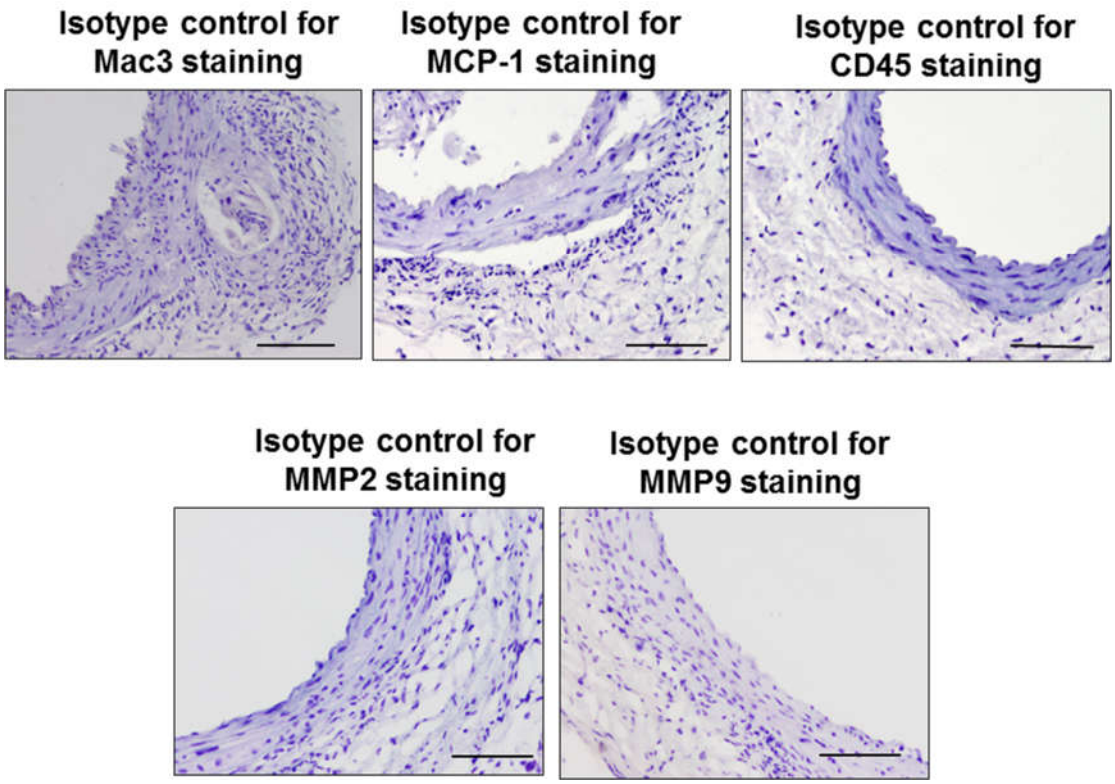

Supplementary Figure XIV. Isotype-specific immunoglobulin negative control for anti-Mac3, anti-MCP-1, anti-CD45, anti-MMP2 and anti-MMP9 primary antibody in aorta. We used hematoxylin (blue) staining to confirm the presence of cells. Bar represents 20 μm.

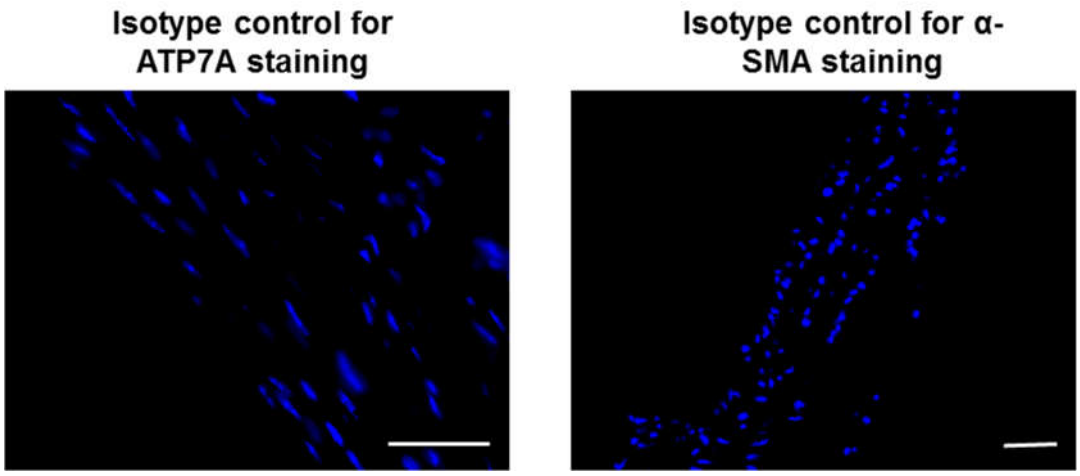

Supplementary Figure XV. Isotype-specific immunoglobulin negative control for anti-ATP7A and anti- α-SMA primary antibody in aorta. We used DAPI (blue) staining to confirm the presence of cells. Bar represents 20 μm.